SYNTHESIS AND CHARACTERIZATION OF PURE AND As_2O_3 SUBSTITUTED BARIUM HEXA-FERRITES

A Thesis Submitted
in Partial fulfilment of the Requirements
for the Degree of
MASTER OF TECHNOLOGY

by

ANUP KUMAR VERMA
Junior Research Fellow
Council of Scientific and Industrial Research
(INDIA)

to the

MATERIALS SCIENCE PROGRAMME
INDIAN INSTITUTE OF TECHNOLOGY, KANPUR

JANUARY, 1989

MSP-1989-M-VER-SYN

To

My Parents

and

Teachers

6.1.89

CERTIFICATE

It is certified that this work "SYNTHESIS AND CHARACTERIZATION OF PURE AND As_2O_3 SUBSTITUTED BARIUM HEXA-FERRITES" by ANUP KUMAR VERMA, has been carried out under my supervision and that this work has not been submitted elsewhere for a degree.

January 2, 1989.

(K.N. Rai)
Professor
Materials Science Programme
and
Department of Metallurgical Engineering
Indian Institute of Technology, Kanpur

ABSTRACT

In the present work the synthesis and characterization of pure and As_2O_3 substituted barium hexa-ferrite have been reported. The As_2O_3 substitution for Fe_2O_3 in $BaO.6Fe_2O_3$ has been presented in terms of mole percent, x and the compositions synthesized cover the composition series $14.3\ BaO.(85.7-x)Fe_2O_3.xAs_2O_3$ with $x \leq 15$ mole percent. The various compositions of ferrite have been prepared using ceramic method and give rise to M-type hexagonal $BaO.6Fe_2O_3$ ferrite particles when they are heat treated from 1100°C to 1300°C. The substitution of As_2O_3 enhances the liquid phase sintering thereby reducing the sintering temperature. The effect of As_2O_3 substitution on structural, electrical and magnetic properties along with sintering condition has been investigated.

The subject matter of this work has been presented in four chapters. Chapter 1 gives a brief introduction to hexa-ferrites and general methods of their preparation. It also covers the crystal structure and the magnetic structure of Ba-ferrite and their electrical and magnetic properties. The dependence of the electrical and magnetic properties on the microstructural properties has been reviewed. Finally the importance of hard ferrites and their possible applications have been described.

The method of preparation and techniques for experimental characterization have been described in Chapter 2. It includes optical microscopy, density measurements, X-ray diffraction analysis, electrical measurements and magnetic measurements. The electrical measurements have been performed for frequency dependence of resistivity, temperature dependence of ac and dc resistivity and frequency dependence of dielectric properties for various compositions synthesized. Magnetic measurements have been carried out for coercivity and specific saturation magnetization.

Chapter 3 deals with the results of the experimental observations and the comparative study of pure and As_2O_3 substituted ferrite compositions. Modifications in X-ray diffraction patterns have been observed with the As_2O_3 substitution. Variation of lattice parameters, c and a, is found to be in good agreement with the variation of half line width and the variation of coercivity of ferrite compositions with As_2O_3. Activation energies for electrical conduction has been determined at different frequencies in the temperature range from 27°C to 500°C. Variation in specific saturation magnetization has been observed with increasing the As_2O_3 content in Ba-ferrite.

Finally the conclusions drawn from the results obtained are included in Chapter 4.

ACKNOWLEDGEMENTS

I take this opportunity to express my deep sense of gratitude to Dr. K.N. Rai for his valuable guidance, critical appraisal and constant encouragement throughout the work.

I am grateful to Dr. S. Ram, ACMS, IIT Kanpur, for his valuable suggestions at the various stages of this investigation.

I wish to thank all technical staff of A.C.M.S. for their cooperation during the course of the experimental work.

I am highly indebted to my friends Messers G.C.Uniyal, Ashok Kumar, Mustaq Ahmed, V. Padmavan, K.M. Dixit and P. Manoravi for their kind help and inspiration.

I would like to thank Mr. U.S. Misra, and Mr.V.P.Gupta for their excellent typing and drawing respectively.

Finally, I sincerely acknowledge the Council of Scientific and Industrial Research, Govt. of India for financial assistance provided to carry out the research work.

-ANUP KUMAR VERMA

Page

LIST OF FIGURES

LIST OF TABLES

CHAPTER 1

SCIENCE OF HEXAGONAL FERRITES

1.1 INTRODUCTION

A large group of ferrimagnetic oxides exhibit hexagonal crystal structure of considerable similarity and they include both hard and soft magnetic materials. Depending upon the similarity of the chemical composition and crystal structure, these ferrites are named as W-type, Y-type, Z-type etc. Their chemical composition is given in Table 1.1. Their chemical composition diagram is also shown in Fig. 1.1. Of these only the hard ferrites having phase composition $BaFe_{12}O_{19}$, $SrFe_{12}O_{19}$ or $PbFe_{12}O_{19}$ type as well as their solid solutions, e.g. $Ba_{1-x}Sr_xFe_{12}O_{19}$ are of considerable economic importance, and are called M-type hexa-ferrite [1]. These are dealt with in great detail in this chapter.

The compound $BaO.6Fe_2O_3$ ($BaFe_{12}O_{19}$) is called barium hexaferrite and it falls in the category of M-type ferrites. It is also denoted as BaM. The properties of this ferrite can be altered by chemical substitution of various ions without disturbing the charge neutrality condition and crystal structure. Substitution for Ba^{2+}, Fe^{3+} and O^{2-} in the compound $BaO.6Fe_2O_3$ is possible. In all the cases, substituted

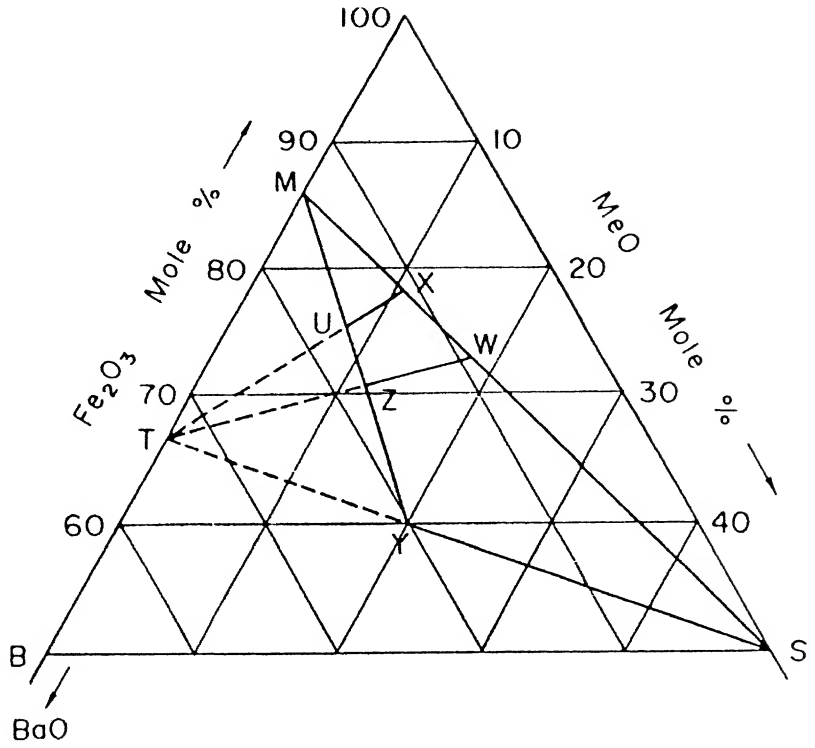

Fig. 1.1 : BaO-MeO-Fe_2O_3 system, showing the relationship of chemical compositions among ferrimagnetic hexagonal compounds (See Table 1.1).

Table 1.1

Chemical Compositions of Hexagonal Compounds in $BaO-MeO-Fe_2O_3$ Systems

Symbol	Crystallographic building up per unit cell	Number of molecules per unit cell	Chemical formula		Composition (mol%) MeO	BaO	Fe_2O_3
S			$MeO-Fe_2O_3$	($MeFe_2O_4$)	50	-	50
T			$BaO.2Fe_2O_3$	($BaFe_4O_7$)	-	33.33	66.67
B			$BaO.Fe_2O_3$	($BaFe_2O_4$)	-	50	50
M	RSR*S*	2M	$BaO.6Fe_2O_3$	($BaFe_{12}O_{19}$)	-	14.29	85.71
W	RSSR*S*S	2MeW	$2MeO.BaO.8Fe_2O_3$	($Me_2BaFe_{16}O_{27}$)	18.18	9.09	72.71
Y	3(ST)	3MeY	$2MeO.2BaO.6Fe_2O_3$	($Me_2Ba_2Fe_{12}O_{22}$)	20	20	60
Z	RSTSR*S*T*S*	2MeZ	$2MeO.3BaO.12Fe_2O_3$	($Me_2Ba_3Fe_{24}O_{41}$)	11.76	17.65	70.59
X	3(RSR*S*S*)	3MeX	$2M3O.2BaO.14Fe_2O_3$	($Me_2Ba_2Fe_{28}O_{46}$)	11.11	11.11	77.78
U	RSR*S*T*S*	MeU	$2MeO.4BaO.18Fe_2O_3$	($Me_2Ba_4Fe_{36}O_{60}$)	8.33	16.67	75.00

*180^{o} rotational symmetry around the hexagonal c-axis.

ions should be so chosen as to maintain the charge neutrality condition and to have similar ionic radii as that of the original ions (Appendix A).

The Ba^{2+} may be substituted partly or completely by Sr^{2+} [2] and Pb^{2+} [3] or by combination, for instance of Ag^{1+} and La^{3+} or Na^{1+} and La^{3+}.

The substitution of Fe^{3+} in BaM will result in the ferrite of chemical formula $BaA_xFe_{12-x}O_{19}$, where A is the element having valency 3+. For example, the subsitution of Al^{3+}[4,5], Ga^{3+} [4,5], Cr^{3+} [4,5], In^{3+}, Sc^{3+}[6] etc. for Fe^{3+} has been extensively studied. Due to the interest in the effect of substituted ions on the magnetic properties of M compounds, attempts to replace Fe^{3+} by non-magnetic ions is reported occassionally, for instance, Bi^{3+} [7,8]. As As^{3+} is also a non-magnetic ion, an attempt to study the effects of As^{3+} substitution has been made in the present work.

1.2 GENERAL METHODS OF FERRITE PREPARATION

There are various processes used to prepare the polycrystalline ferrites. The size, shape and distribution of grains and pores throughout the material, varies with different synthesizing techniques, firing temperatures, sintering times and atmosphere. Some of important methods are given below.

1.2.1 Oxide Method

In this method the ferrite in the form of powder or in a sintered polycrystalline state is obtained by the solid state reaction by heating the mixture of constituent oxides. Solid state reaction depends on the particle size, temperature, sintering time, chemical nature, and crystal structure of the reactants. Wet ball milling is done by using stainless steel balls for the fine mixing of powders. Then mixture is dried and pressed into pellets using polyvinyl alcohol as a binder. Some times pellets are crushed after presintering to obtain better homogeneity of material. To increase the coercivity, magnetic field is applied to orient the grains of the material in a particular direction during pelletization. High temperature sintering results in grain growth and consequent reduction in coercivity.

1.2.2 Decomposition Method

In this method, instead of using oxides as starting materials, their oxalates, sulphates, chlorides, nitrates or hydroxides are used. Thus oxides are formed by thermal decomposition while sintering.

1.2.3 Coprecipitation Method [9,10]

To avoid the lengthy milling processes involved in wet milling, attempts have been made to simultaneously

precipitate the required hydroxides from solution, so that precipitate containing the required metals in correct proportions, which are already intimately mixed, is obtained. Knowledge of the solubility product of the substances is essential in order to determine the pH value for complete precipitation. The mixed cations are precipitated out by a strong base (usually NaOH) in a specific pH and dilution range. The pH is also related to solubility product. The most important feature of this method is the intimate mixing of ions on the atomic level, so that subsequent nucleation and crystallization can occur at low temperatures. This behaviour prevents grain growth and the particles are perfect in that they are free from stresses and strains caused by particle diminution in milling. High coercivity thus can be expected from this method.

1.2.4 Electrolytic Co-precipitation Method

In this method, the composition is formed by electrolysis from the anode, which is made of metal. Type of metal would depend on the oxide required.

1.2.5 Hot Pressing [11]

High quality permanent magnetic materials are also prepared by pressing very fine ferrite powders at high temperatures. For this process, pressure and temperature are to

be optimized to reduce particle size, so that coercivity of the materials may increase.

1.2.6 Other Methods

Single crystals of pure and substituted $M.Fe_2O_3$ (M-Ba,Sr) have been grown from different solvents by spontaneous nucleation growth [12] . Strong improvement in crystal size was obtained using Na_2O-Fe_2O_3 flux. Thin film deposition methods are also employed for Ba-ferrite [13].

1.3 STRUCTURE AND PROPERTIES OF FERRITES

1.3.1 Crystal Structure

The BaM, SrM and PbM are all hexagonal type ferrite and possess the same crystal structure as mineral magnetoplumbite, $PbO.6\ (Fe_{1.25}\ Mn_{0.6}\ Al_{0.8}\ Ti_{0.08})_2O_3$. In case of pure Barium hexaferrite, Fe^{3+} ions occupy the same crystallographic positions as the mixtures of Fe, Mn, Al and Ti in the mineral magnetoplumbite [14] . Figure 1.2(a) is a perspective drawing of BaM crystal structure. Ba^{2+} and O^{2-} are large and have nearly the same atomic radii (Appendix A). These ions therefore form a close packing of ABAB....or ACAC.... type perpendicular to [00.1] axis (c or z-axis) of ferrite lattice, as shown by atomic layers 2,3,4,5,6,8,9,10,11,12 in Fig.1.2(a). This stacking sequence can also be written as hhhkkhhhkk in Jagodzinski symbol and as (113 113) in Zhadnov symbol [15].

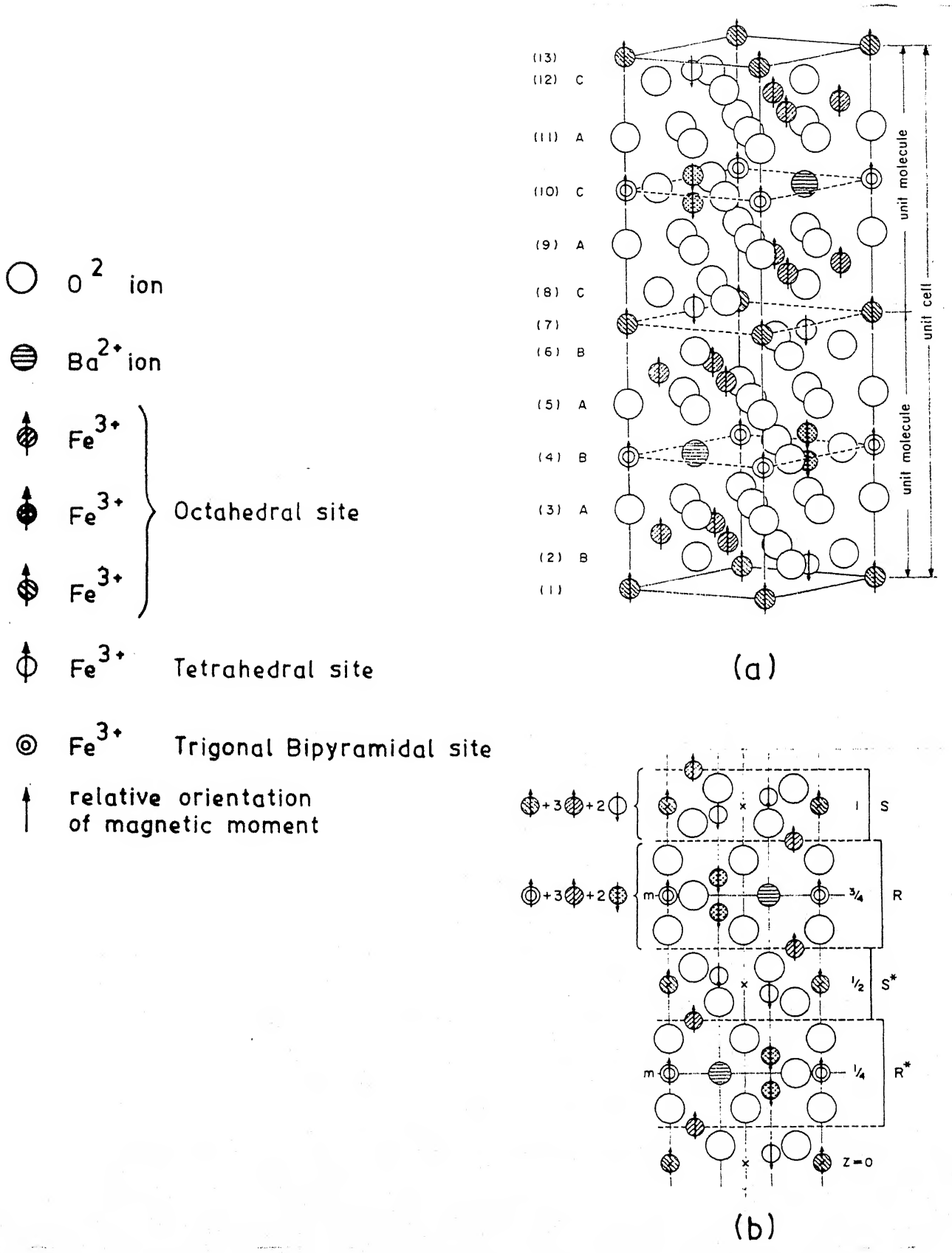

Fig. 1.2 (a) Perspective drawing of $BaO \cdot 6Fe_2O_3$
(b) The (110) section of $BaO \cdot 6Fe_2O_3$

The smaller Fe^{3+} ions are located in the interstices. The unit cell consists of 10 close packed layers. The eight close packed layers consists of purely O^{2-}, and the remaining two layers (4&10) consist of three oxygen and one barium ion, i.e., in every fifth oxygen layer, one O^{2-} is replaced by Ba^{2+} (Sr^{2+} or Pb^{2+}) in BaM (SrM or PbM) respectively. This occurs due to similarity of their (Ba^{2+} and O^{2-}) ionic radii, Five oxygen layers (including Ba^{2+} at 4 and 10) make one molecule and two such molecules make one unit cell. The unit cell as a whole has hexagonal symmetry with $a = b = 5.89$ Å and $c = 23.2$ Å. The upper molecule (layers 7 to 13) shows 180^{o} rotational symmetry around the hexagonal c-axis against lower molecule (layers 1 to 7). The O^{2-} layer containing Ba^{2+} is a mirror plane, being perpendicular to the c-axis. The filling of interstitials in hexaferrite by Fe^{3+} ions is identical to that of spinels. Fe^{3+} ions occupy the interstitial positions of oxygen lattice. The space group of the compound is denoted by $P6_3/mmc$ [1]. Each layer consists of 4 large ions. Thus the oxygen and barium ion close packed lattice consists of three types of interstitials namely, tetrahedral (surrounded by four O^{2-}), hexahedral (surrounded by five O^{2-}, three on the bottom and two on the top) and octahedral (surrounded by six O^{2-}).

Figure 1.2(b) represents the 110 section of BaM. It shows the atoms and symmetry elements in a mirror plane containing the c-axis [16] . S and R are the building blocks of the crystal, and S* and R^* indicate the blocks obtained by rotating S and R through 180° about the c-axis, as previously illustrated. Thus the unit cell of BaM can also be expressed as $RSR^*S^*[1]$.

1.3.2 Magnetic Structure

In M-type compounds, the magnetic ion Fe^{3+}, has typical ferrimagnetic structure. That is, the orientation of the magnetic moments of the ferric ions in the crystal are generally aligned along the c-axis in antiparallel direction with each other. The arrows in Fig. 1.2 (a) and Fig.1.2(b) represents orientation of magnetic moment of Fe^{3+} as a result of superexchange interaction. Each unit cell consisting of two molecules of barium ferrite has 24 Fe^{3+} ions, with the distribution of six Fe^{3+} ions in each blocks R,S,R^* & S^*. It is clear from the Fig.1.2 that the S block contains four Fe^{3+} with spin-up in octahedral sites and two Fe^{3+} with spin-down in tetrahedral sites. In the R block, there exist three Fe^{3+} of spin-up orientation in octahedral sites, two Fe^{3+} of spin-down orientation in octahedral sites and one Fe^{3+} of spin-up orientation in a trigonal bipyramid site (hexahedral site) [1]. Thus in a molecule of $BaFe_{12}O_{19}$, the arrangement of magnetic ion is -

Hexahedral sites	-	1(↑)
Octahedral sites	-	7(↑) + 2(↓)
Tetrahedral sites	-	2(↓)
		8(↑) + 4(↓)

Since every Fe^{3+} has the magnetic moment of $5\mu_B$ at 0^oK, the magnetic moment of one molecule of barium ferrite will be $5x4\mu_B = 20\mu_B$. Therefore magnetic moment per unit cell of BaM is $2x20\mu_B = 40\mu_B$. The theoretical saturation magnetization (M_s) and specific saturation magnetization (σ_s). thus can be calculated as follows:

$$M_s = \frac{\text{magnetic moment of the unit cell}}{\text{volume of the unit cell}}$$

$$M_s(0^oK) = \frac{40 \times 0.927 \times 10^{-20}}{6.94 \times 10^{-23}} \text{ ergs/Oe-cm}^3$$

$$= 538 \text{ emu/cm}^3$$

$$\therefore \sigma_s = \frac{M_s}{\text{Density}} = \frac{538}{5.28} = 101 \text{ emu/gm}$$

Saturation magnetization decreases approximately linearly with temperature. At $T = 20^oC$, $\sigma_s = 72$ emu/gm.

1.3.3 Magnetic Properties

The usefulness of a permanent magnet is determined by the magnetic energy it delivers at various flux densities. Since the magnetic potential energy of the magnetized material is approximately equal to BH/2. The maximum energy product $(BH)_{max}$ is however one of the main criteria for the characterisation of permanent magnets (Fig. 1.3) [17]. Other useful parameters are M_s, the saturation magnetisation, H_c, the coercive field, M_r, the remanent magnetization, T_c, the Curie temperature and the hysteresis. The origin of these properties and their variation, depend on the material, method of its processing and other physical factor.

(a) Saturation Magnetization

It is the maximum value of magnetization for a ferromagnetic or ferrimagnetic material (Fig. 1.3). Sometimes the term specific (saturation magnetization (σ_s) is used which is the total magnetic moment per unit mass. Its unit is emu/gm or gauss. cm^3/gm in cgs system. Saturation magnetization decreases with increase in milling time of initial raw mixture, owing to formation of soft magnetic phase. It can be overcome by annealing the sample [18]. Higher the M_s value higher will be the energy product, (BH).

(b) Remanent Magnetization

After removal of magnetic field, the remaining magnetization in the sample is known as remanent magnetization (Fig.1.3).

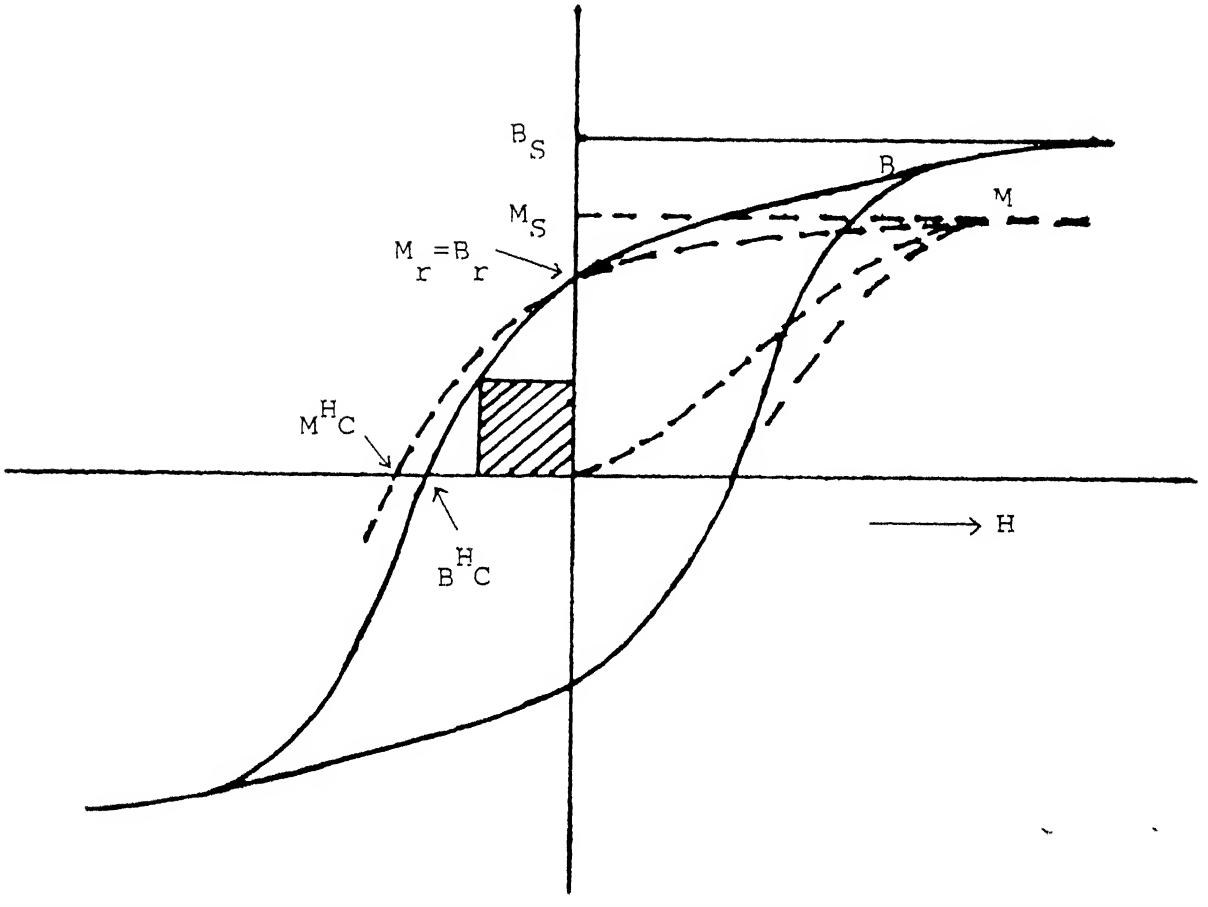

Fig. 1.3 : Saturation hysteresis loop for magnetic flux density B as a function of H (drawn) and for magnetisation M as a function of H with initial magnetisation curve (dashed). The shaded area is equal to the maximum energy product $(BH)_{max}$)

Remanence can be increased considerably by pelletising the powder in a magnetic field before sintering [19] .

(c) Coercivity

Coercivity is defined as the field applied in reverse direction to demagnetize a specimen (Fig.1.3). It is proportional to M_r value. The various factors affecting the coercivity are as follows:

(i) Particle Size

The larger the particle size, the more the number of domains in it and vice versa. During the process of magnetisation and demagnetisation, motion of domain walls is easier than that of rotation of magnetic moments (rotational magnetisation). Thus, in general, larger the size of particles the smaller the magnetic field required to demagnetize it, i.e., H_c will be smaller. However, when we decrease the material dimensions below some critical size, we encounter strikingly different behaviour associated with domain structures and magnetisation is unique to fine particles. Domain boundary motion ceases to play a significant role because the particle becomes too small to contain domain boundaries. Radical changes in permeability and coercivity are then observed [20a].

For single domain particles there are three general ways by which the particles can reverse their magnetisation under the influence of demagnetizing field 20b .

(a) By domain rotation

(b) By changing the single domain structure, i.e., by promoting nucleation and growth of a reverse domain

(c) By curling in the domain on itself to produce a flux configuration normal to the applied field.

Any of these processes can decrease the coercive force drastically.

(ii) Crystal Anisotropy

In the absence of other influences the magnetisation vector of a spherical single domain particle is directed along an easy crystallographic direction to minimize the magnetocrystalline anisotropy energy. To rotate the magnetisation vector along a more difficult crystal direction requires application of a reverse field (H_c) which is equal to $2K/M_s$ [20c], where K is the constant of magnetocrystalline anisotropy and M_s is the saturation magnetisation. So the higher the anisotropy energy, the higher will be the coercive force.

(iii) Strain Anisotropy

It has been observed that the mechanical strain increases the coercive force of a single domain particle by $\frac{3\lambda T}{M_s}$, where λ is the magnetostriction constant and T the applied stress. This

effect is quite similar to that of crystal anisotropy. In order to rotate its magnetization vector the particle must pass through a region of high anisotropy with respect to the stress [20c] .

(iv) Shape Anisotropy

An elongated single domain particle free from crystal or strain anisotropy will direct its magnetization vector along a major axis where the demagnetizing factor is a minimum and magnetostatic energy is therefore the lowest. This effect has been exploited in case of metallic magnetic like 'Alnico', ESD magnets [20c].

(d) Hysteresis

The word 'hysteresis' is Greek, meaning "a coming late", and is today applied to almost any phenomenon in which the effect lags behind the cause. In an external magnetic field, the favourable oriented domains grow at the expense of those aligned unfavourably to the field. Finally at larger fields, all domains are oriented parallel to the field due to rotation of magnetisation vectors. Upon the removal of external saturating magnetic field in reverse direction, the same path will not be traced. This is due to irreversible domain wall movements, causing the phase lag between external field and magnetisation, leading to an open loop [21]. A hysteresis is shown in Fig. 1.3 . The total heat generated during one cycle

of hysteresis, which is measured by the area enclosed by the hysteresis loop, is equal to the total energy dissipated by discontinuous magnetisation processes.

(e) Curie Temperature

It is the temperature at which spontaneous magnetisation of ferrite vanishes. That is the material becomes paramagnetic above Curie temperature. This is because, the ordering tendency of exchange energy is opposed by disordering effect of thermal energy.

(f) Magnetic Losses in Ferrites

Various types of losses occur in ferrites like electrical, magnetic, mechanical etc. These losses cause undue excessive heat, which decreases the life of device and other effects like sensitivity, increased attenuation etc. also come into play. Therefore for device purpose, the material should have as low level of losses as possible. Magnetic losses are quite significant in the magnetic devices. The magnetic losses are mainly due to following factors [22]:

(i) Eddy Current Loss

This loss is directly proportional to the square of the frequency (f^2) and independent of the field strength (H).

It is quite small in BaM type compound owing to their high resistivity.

(ii) Hysteresis Loss

It is due to property of hysteresis of magnetic material. It is the function of both frequency (f) and field strength (H).

(iii) Residual Loss

It is due to domain wall relaxation and domain rotation resonance. It is frequency dependent and independent of applied magnetic field (H).

So total loss tangent may be written as

$$\tan \delta_m = \tan \delta_h + \tan \delta_f + \tan \delta_r$$

(total loss) (hysteresis loss) (eddy current loss) (residual loss)

Then quality factor is

$$Q = \frac{1}{\tan \delta_m}$$

1.3.4 Electrical Properties

The resistivity of ferrites is sufficiently high so eddy current losses could be neglected for most of the low

frequency applications. At microwave frequencies, however, dielectric losses determine in many instances, the limiting performance of ferrite devices.

The electrical properties of a polycrystalline ferrite may vary markedly, depending upon the heat treatment given to it during preparation. The oxygen dissociation pressure over Fe_2O_3 of a $MO.6Fe_2O_3$ increases rapidly above 1200°C. This may lead to the formation of some divalent iron (FeO). The presence of Fe^{3+} and Fe^{2+} ions in the same lattice grid leads to electrical conductivity due to electron hopping mechanism [23]. If the material is cooled in an oxygen atmosphere it may lead to formation of high resistivity thin film around grain boundaries. It occurs due to fast migration of oxygen ion through pores and grain boundaries resulting in oxidation of divalent iron. This imparts inhomogeneous dielectric structure to ferrites. Koops [24] explained the inhomogeneous dielectric behaviour of ferrites (Appendix B). As these have been fired and cooled under different conditions, these differ in Fe^{2+} contents and hence differ in electrical properties.

The specific resistivity ρ of ferrites is many orders of magnitude higher than that of metallic magnetic materials. Commercial ferrite specimens usually have a dc resistivity of at least 10^6 Ω-cm at room temperature [25].

Thermally activated nature of conduction mechanism in ferrites is similar to that of semiconductors, i.e., their electrical resistance drops with rising temperature and hence the temperature dependence of specific resistivity (ρ) can be written as [26]

$$\rho = \rho_o \exp (Q/kT)$$

where ρ , specific resistivity at T ^oK

ρ_o , specific resistivity at 0^oK

Q , activation energy for electrical conduction mechanism

k , Boltzmann constant.

'Q', the activation energy for electrical conduction is found from the slope of log ρ vs. $10^3/T$ plot. Temperature dependence plot of electrical resistivity for ferrites shows different slopes in different temperature region. Each slope corresponds to a particular type of conduction mechanism dominant in that region

1.4 IMPORTANCE OF HARD FERRITES AS PERMANENT MAGNETIC MATERIALS

The potential suitability and actual use of any material for a specific purpose depends on a number of

physical and economic factors. Hard ferrites are widely used as permanent magnetic materials due to following factors:

(i) Magnetic Saturation

Magnetic saturation at least up to room temperature and above room temperature, is not much, but is comparable to other permanent magnetic materials. Value of saturation flux density for Ba-ferrite at room temperature is ~3.80 K Gauss [27]. It is thus considerably lower than that of iron (21.5 K Gauss) or that of Alnico alloys (~ 14.0 K Gauss).

(ii) Coercivity

At room temperature coercivity upto 6 KOe has been found in very fine particles about 0.1 μm [28]. In commercial specimens the crystallites are present in sizes of about 1μm, and only smaller $_{J}H_{C}$ (coercive field) values are attained. However it is attractively high enough for a large number of applications. It is appreciably higher than that of the Alnico materials (~ 1.2 KOe) commonly used.

(iii) Stability of Material

In a number of materials the structure at room temperature is in a 'frozen' metastable state which by diffusion or allotropic transformation can change towards equilibrium as a result of a temperature rise. This has an adverse effect on the magnetic values, specially the coercivity. This phenomenon is termed as 'structural ageing' which in most

materials occurs far below the Curie temperature and thus imposes restrictions on the actual use of the magnets. However hard ferrites are an exception in this respect. Their structure remains stable for beyond the Curie temperature. And in case of Ba- and Sr- based hard ferrites structure and chemistry remains unchanged even above 1400°C (in air) before oxygen is released and phase transformation occurs [29].

Chemical stability prevails when the material does not react with the ambient medium. Naturally, the type of reaction and its extent depend on the medium. As the cations of the $BaFe_{12}O_{19}$ and $SrFe_{12}O_{19}$ lattices are in the highest state of oxidation, these materials are stable which is an advantage over metallic materials.

(iv) Economic Viability

The cost of materials and production are lower for hard ferrites than for other grades of permanent magnets if related to the same energy content. A number of favourable circumstances as discussed further made them industrially important.

The raw materials required for inexpensive, abundantly available and easy to handle. Extreme purity is not necessary. Iron oxides having 0.5 to 1 percent by weight of impurities, and natural hematite (α-Fe_2O_3) or iron oxides from waste can also be used.

The temperature necessary for the raw materials to react to form ferrite (calcination) and for sintering are normally around 1200°C to 1300°C. Both processes take place in air, while with metal powders a protective atmosphere or vacuum is always required.

For the high grade ferrites a powder consisting of single-domain particles in sizes of 1 µm or less is needed, a fineness which can easily be adjusted by grinding in water. With metal powders, however, water would not be suitable as a grinding medium so as a rule organic liquids are used. This in view of pollution and health hazards is more difficult to handle.

The ferrite powder is generally shaped by one-sided or two-sided pressing in a die and the plastoferrites by injection moulding, calendering etc.

1.5 APPLICATIONS OF HARD FERRITES

Hard ferrites have wide field of application as a permanent magnet throughout the world. These are widely used in electrical engineering in electrical to mechanical energy conversion, mechanical-to-electrical energy conversion and microwave applications. Barium ferrite magnets are used for oil filters, electric generators, permanent magnet motors, loudspeakers, moving-coil instruments etc. Low magnetisation and high coercivity of these materials make these specially suitable for applications where large demagnetising fields are encountered [17] .

These ferrites find only limited applications in recording surfaces, primarily because of their high coercivity. It requires erasing and recording head with high saturation flux density. However, the high coercivity of these materials gives the recording surface a unique ability to withstand, high demagnetising fields (erasing fields). This property has been utilized specially for the two major applications. In the first application master tapes are made from high coercivity hard ferrites which are used to transfer information in copying tapes by bringing two tapes master tape and copy tape) together in presence of a magnetic field. Other application is in magnetic strikes on credit cards and magnetic badges.

Owing to their high resistivity and large uniaxial magnetocrystalline energy, these ferrites are used in microwave communications and radar system as high frequency resonant devices such as tunable filters, gyrators and isolators etc. Again these magnets possess low eddy current losses therefore they are suitable for making a polarising pulse transformers, polarised relays, microphones and telephone circuits [30].

These ferrites are particularly found to be suitable in the area of magnet mechanics where the forces set up by magnetic fields are utilized for adhesion, attraction, repulsion, damping, rotating etc. For example they are used

as magnetic chucks to hold work piece during grinding, milling, plaining and turning [17].

Bonded hard ferrites are the composite materials in which hard ferrite powder is embedded in a non-magnetizable matrix. Mostly organic materials are used for the matrix on a large scale, for e.g., rubber, polyvinylchloride (PVC), polyamides (PA), polyolefins (e.g. polyethylene and polypropylene), polysterene, phenol and polyester resins [31]. These ferrites bonded with organic matrix, are also called plastic bonded hard ferrites or simply, plastoferrites. Inorganic matrix used are metal and glass [32].

Since the volume proportion of the magnetic phases is smaller than in the pure compact hard ferrites, reduced magnetic properties are encountered in plastoferrites. The bonded hard ferrites are therefore only used for those applications where relatively low magnetic level is required. Since these are the plastic based composites, it makes it possible to use the advantageous forming methods known in plastics technology and to impart various shapes and elasticity. For example these are used in refrigerator doors, gaskits, magnetic belts etc. [33].

CHAPTER 2

EXPERIMENTAL PROCEDURE

2.1 SYNTHESIS OF PURE AND As_2O_3 SUBSTITUTED BARIUM HEXA-FERRITE

2.1.1 Raw Materials

The details of raw materials used, in the present investigation, for the preparation of barium hexa-ferrite are tabulated below:

Material	Manufacturer	Quality
Fe_2O_3 powder	Thomas Baker and Co., Bombay (India)	AR Grade
$NaHCO_3$ powder	Glaxo Laboratories (India) Ltd., Bombay	LR Grade
$BaCl_2.2H_2O$ crystals	Sarabhai M. Chemicals, Baroda (India)	GR Grade
As_2O_3 powder	V.O. Sojuzchimckpory, Moscow (USSR)	LR Grade

2.1.2 Preparation

(a) Chemical Processing

In the present work barium carbonate ($BaCO_3$) was obtained by precipitating it from the aqueous solution of sodium bicarbonate ($NaHCO_3$) and barium chloride ($BaCl_2.2H_2O$) according to following chemical reaction:

$$BaCl_2.2H_2O + 2NaHCO_3 \longrightarrow BaCO_3 \downarrow + 2\ NaCl + 3H_2O + CO_2\uparrow$$

The aqueous solution of desired concentration of sodium bicarbonate and barium chloride were made separately. The barium chloride solution was first soaked in iron oxide (Fe_2O_3) powder. The sodium bicarbonate solution was added to it slowly. As a result barium carbonate was intimately precipitated on iron oxide particles leading to a better chemical homogeneity. Aqueous solution of arsenic oxide (As_2O_3) was made in hot water and added to above mixture in desired proportion. Finally the mixture was filtered and dried.

(b) Wet-milling and Pelletization

The above mixture was milled in water media using a rotating steel lined planetary ball mill with tungsten carbide balls (2:1 proportion by weight) for 4 hours. After wet milling, the slurry mixture was dried at 100°C followed

by grinding in mortar pestle to obtain fine powder and pelletization of the powder into cylindrical form (dia - 1.2 cm, length - 1.0 cm) using hydraulic press at a pressure of 4 tonnes/sq.inch.

(c) Ferritization

Pelletised samples were then sintered for ferritization at 1100°C, 1200°C and 1300°C for 6 hrs and 20 hrs, in globular furnace.

The possible chemical reaction during sintering is given below [34]:

$$BaCO_3 + Fe_2O_3 \xrightarrow{T < 750^\circ C} BaO.Fe_2O_3. + CO_2$$

$$BaO.Fe_2O_3 + 5Fe_2O_3 \xrightarrow{T > 850^\circ C} BaO.6Fe_2O_3$$

2.1.3 Composition of Prepared Ferrites

The ingredients ($BaCO_3$, Fe_2O_3 and As_2O_3) were mixed in such a ratio as to yield ferrites of composition series 14.3 BaO. (85.7-x) Fe_2O_3.xAs_2O_3, where x = 0,1,2,3,5,10 and 15. The sample notations and their compositions are given in Table 2.1

Table 2.1

Composition of prepared ferrites

Sl.No.	Composition formula	Sample code	Contents (mole percent)		
			BaO	Fe_2O_3	As_2O_3
1.	14.3 BaO-85.7Fe_2O_3	A0	14.3	85.7	0
2.	14.3 BaO-84.7Fe_2O_3-1As_2O_3	A1	14.3	84.7	1
3.	14.3 BaO-83.7Fe_2O_3-2As_2O_3	A2	14.3	83.7	2
4.	14.3 BaO-82.7Fe_2O_3-3As_2O_3	A3	14.3	82.7	3
5.	14.3 BaO-80.7Fe_2O_3-5As_2O_3	A5	14.3	80.7	5
6.	14.3 BaO-75.7Fe_2O_3-10As_2O_3	A10	14.3	75.7	10
7.	14.3 BaO-70.7Fe_2O_3-15As_2O_3	A15	14.3	70.7	15

2.2 CHARACTERISATION TECHNIQUES

2.2.1 Optical Microscopy

Microstructure studies of specimen in relation to As_2O_3 addition and heat treatment were carried out using optical microscopy. The samples were polished using successive grade of emery papers followed by wet wheel polishing with water - Al_2O_3 (0.5 mm) slurry. The Zeiss optical microscope was used at magnification 800 and 320

in white light to record the microstructures.

2.2.2 Density Measurements

The sintered density determination was done by liquid immersion method with distilled water as medium. The samples were dried in the oven at 150°C in order to remove moisture and any other trapped gaseous materials. The initial dry weights (W_1) of the samples were taken with an electrical balance. The samples were then immersed in a beaker containing distilled water and boiler for two hours to allow the water to enter the pores of samples by replacing the trapped air bubbles. The samples were removed and blotted gently. The saturated weight (W_2) of pellets in air and in distilled water (W_3) was measured and the density (ρ) was calculated using the formula:

$$\rho = \frac{W_1}{W_2 - W_3}$$

2.2.3 X-ray Diffraction Analysis

The X-ray diffraction patterns of the samples in the pellet form were recorded using Siefert Iso-Debyflex 2002 diffractometer. The target used was CrKα (λ= 2.291002 Å). The following diffraction parameters were set while recording the X-ray diffraction patterns.

Tube voltage - 40 KV

Tube current - 35 mA

Counts per second (cps) = 100

Time constant - 10 seconds

Scanning rate - 3.0°/min

Chart speed - 60 mm/min.

The diffraction patterns recorded were used for further analysis. The 2θ values and half intensity line widths were measured very accurately. The d values were calculated using Bragg's relation: $2d\sin\theta = \lambda$. Corresponding (hkl) values were noted from the standard ASTM X-ray diffraction file.

Lattice parameters, c & a were calculated susing formula:

$$\frac{1}{d^2} = \frac{4(h^2 + hk + k^2)}{3a^2} + \frac{l^2}{c^2}$$

2.2.4 Electrical Measurements

The sintered cylindrical pellets of approximately 1 cm in length and 1.2 cm in diameter were silver painted on their flat surfaces to get ohmic contacts. The resistance (R) in series mode, capacitance (C_p) and dissipation factor ($\tan\delta$) in parallel mode were measured at different frequencies using an impedence bridge (Model 1608A),

supplied by General Radio Company, U.S.A. A.C. resistance and D.C. resistance of the samples were also measured at different temperatures, viz. 27°C to 500°C.

The sample holder used for the electrical measurement is shown in Fig. 2.1. The electrical parameters were determined as follows:

(a) Resistivity Determination

The resistivity was calculated using the formula [35]:

$$\rho = R \times \frac{A}{L}$$

where,

R, resistance of the pellet

A, area of cross-section of pellet

L, length of the pellet.

(b) Dielectric Constant and Dielectric Loss Determination

Capacitance at different frequencies was measured in parallel mode and the dielectric constant (ε') was determined using relation [35]:

$$C_p = \varepsilon_o \varepsilon_p' \times \frac{A}{L}$$

where, C_p, capacitance of the pellet

ε_o, permittivity of the free space

ε_p', dielectric constant of material

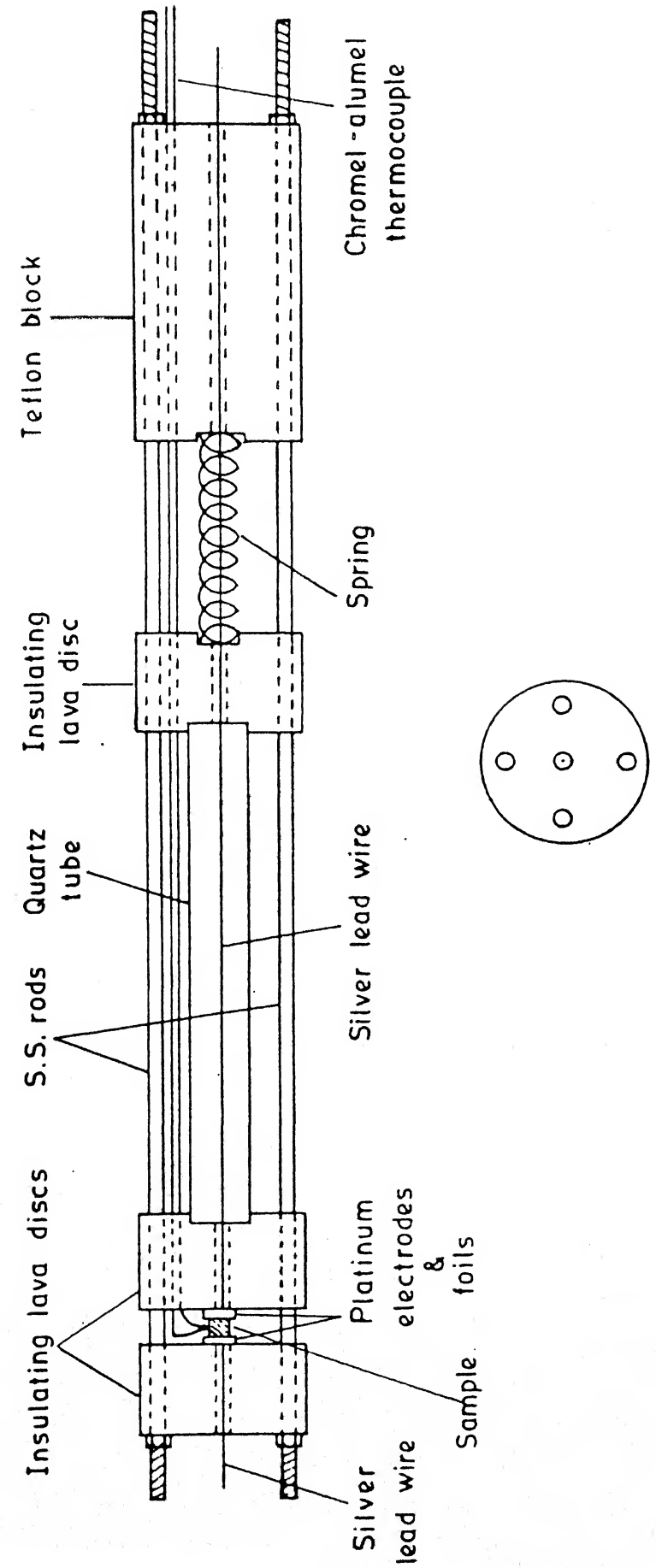

Fig. 2.1 Sample holder for the electrical measurements.

The dissipation factor or loss tangent ($\tan\delta$) was measured at different frequencies and hence dielectric loss (ε''_p) was calculated using formula:

$$\varepsilon''_p = \varepsilon'_p \times \tan\delta$$

(c) Determination of Activation Energy

Resistivity of ferrite samples obey the following relation [26]:

$$\rho = \rho_o \exp(Q/kT)$$

where symbols have their usual meaning.

$$\therefore \ln\rho = \ln\rho_o + \frac{Q}{kT}$$

$$\text{or} \quad \log\rho = A + \frac{Q}{2.303\times10^3 \times k}\left(\frac{10^3}{T}\right)$$

where A is a constant.

Therefore, the activation energy for electrical conduction was evaluated from the slope of the $\log\rho$ vs $10^3/T$ plot. If m is the slope of this plot,

$$m = \frac{Q}{2.303 \times 10^3 \times k}$$

$$\therefore Q = 2.303 \times 10^3 \times k \times m$$

$$\text{or} \quad Q = 2.303 \times 10^3 \times 8.625 \times 10^{-5} \times m \text{ (eV)}$$

$$\text{or} \quad Q = 0.1986 \times m \text{ (eV)}.$$

2.2.5 Magnetic Measurements

The magnetic properties specific saturation magnetization (σ_s) and coercivity (H_c) were investigated for the ferrite samples of spherical shape having radii ∿2 mm, using a parallel field vibrating magnetometer (Model 150A) supplied by the Princeton Applied Research Corporation, New Jersey. The maximum applied field was 12 KOe. The magnetic measurements were done at room temperature.

Specific magnetization (σ) was plotted against the applied magnetizing (+H) and demagnetizing (-H) field. The specific magnetization does not saturate for a magnetic field upto 12 KOe. The reported σ_s values were therefore estimated using the law of approaching to saturation (extrapolation of the plot) [36]. The coercivity values determined were simply the values of demagnetizing field for which $\sigma = 0$.

CHAPTER 3

RESULTS AND DISCUSSION

The results of experimental observations are presented and discussed in this chapter.

3.1 OPTICAL MICROSCOPY

The microstructures of the prepared Ba-ferrites with different As_2O_3 content, sintered at 1300°C for 20 hrs have been shown in Fig. 3.1. It reveals that crystallisation volume fraction and particle size increase with the increase in As_2O_3 content upto 3 mole percent. It implies that the substitution of As_2O_3 in the system induces the formation of $BaO.6Fe_2O_3$ at the expense of iron oxide as per the reaction given below [37]:

$$BaO + 6\ Fe_2O_3 \xrightarrow{As_2O_3} BaO.6Fe_2O_3$$

Thus As_2O_3 acts as a nucleating agent for ferrization. The increase in content of As_2O_3 more than 5 mole percent does not favour the growth of ferrite particles and the ferrite particles disperse homogeneously throughout the material. This could have caused the observed increase in the density of the ferrites.

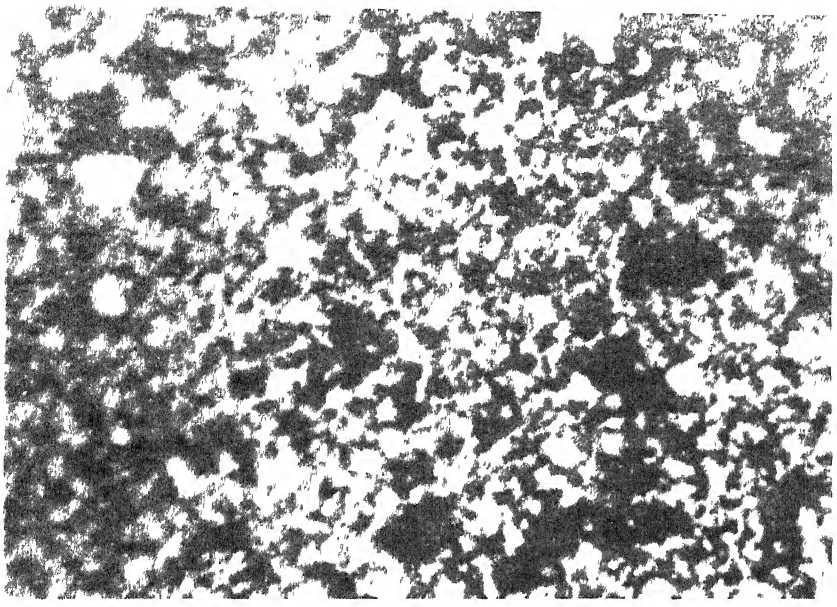

(a) As_2O_3 content = 0 mole percent

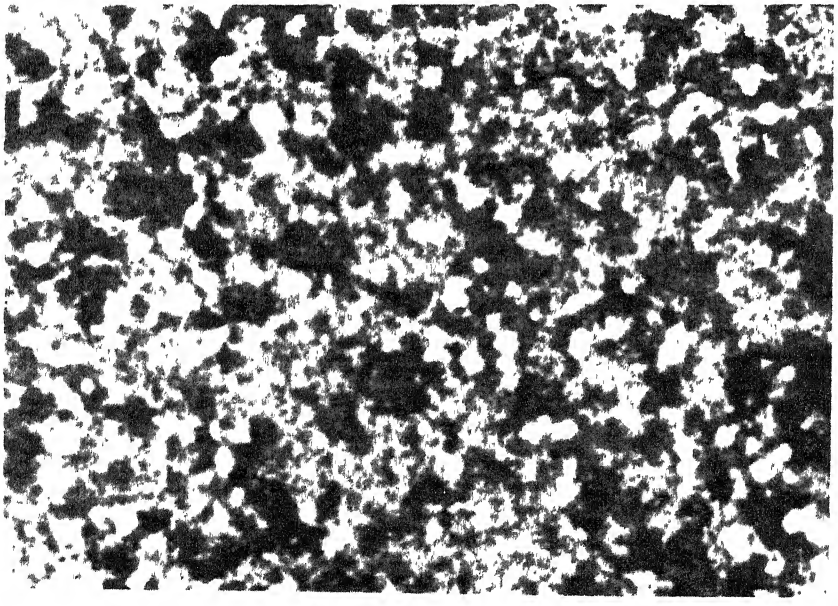

(b) As_2O_3 content = 2 mole percent.

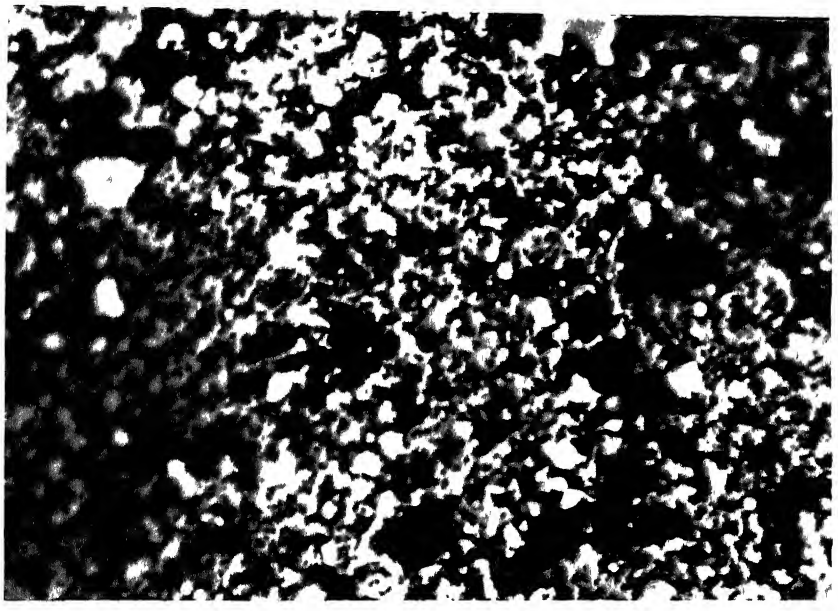

(a) As_2O_3 content = 0 mole percent

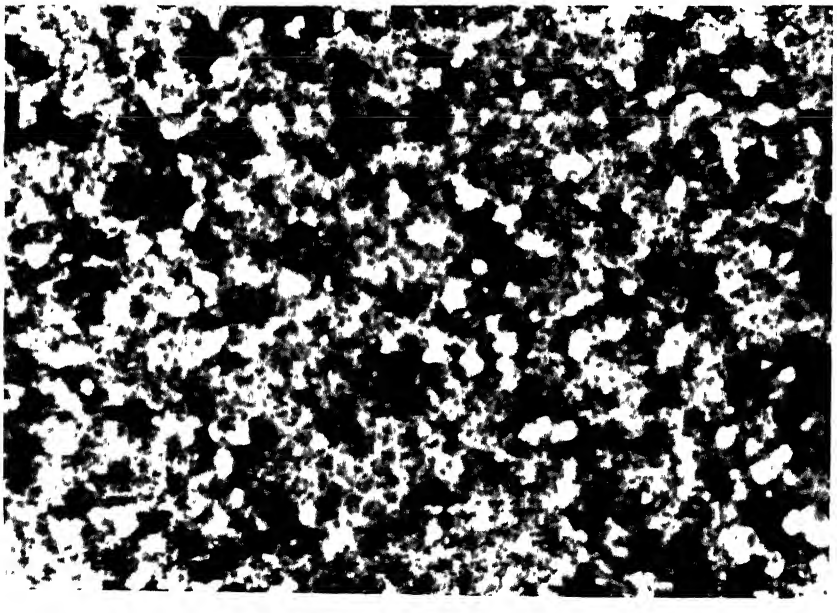

(b) As_2O_3 content = 2 mole percent.

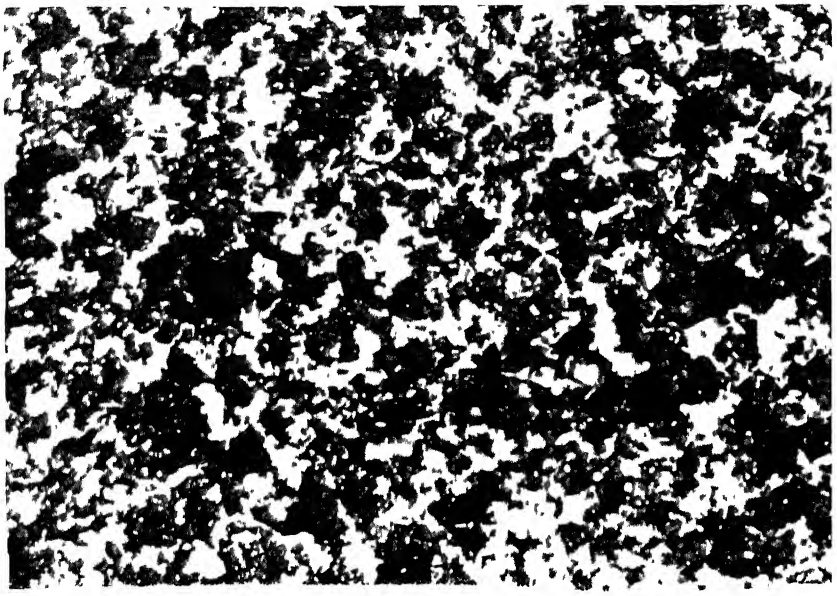

(c) As_2O_3 content = 5 mole percent

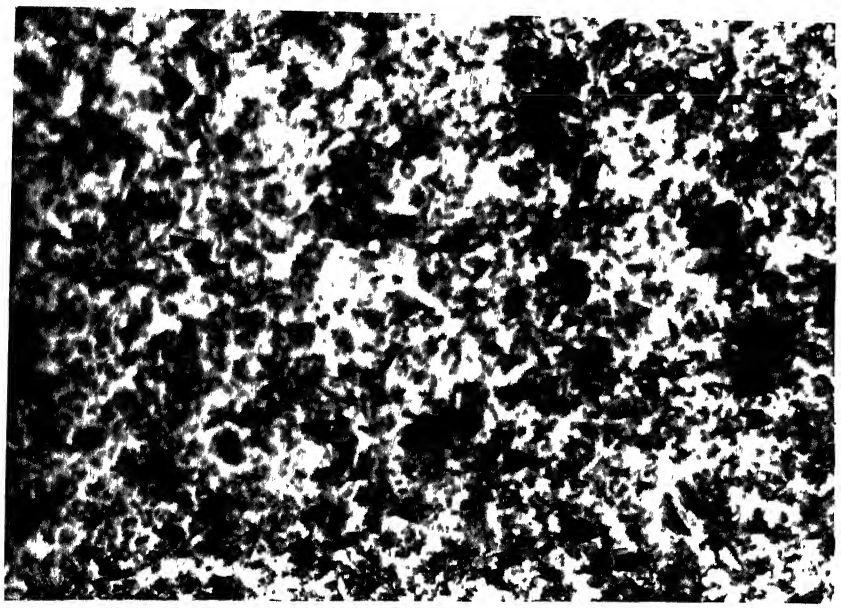

(d) As_2O_3 content = 10 mole percent.

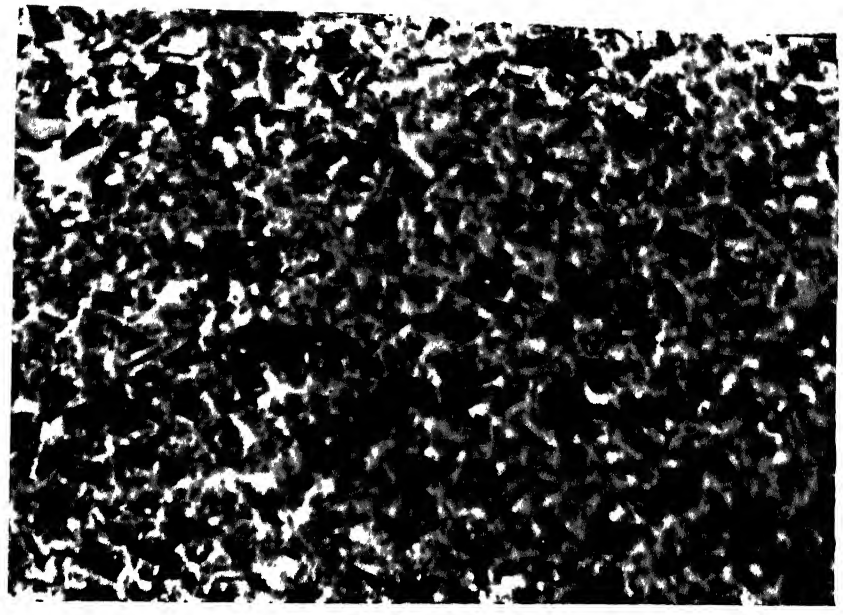

(e) As_2O_3 content = 15 mole percent

Figure 3.1 : Optical Micrographs of Pure and Substituted As_2O_3 Ba-ferrites Sintered at 1300°C for 20 hrs. Magnification 800.

3.2 DENSITY MEASUREMENTS

The variation of density as a function of As_2O_3 content in Ba-ferrite has been plotted in Fig. 3.2. The following observations are worthnoting:

(i) The density of pure ferrite (AO) prepared is low as compared to the X-ray density (5.29 gm/cm^3) [38]. This is due to its porosity.

(ii) The density of the As_2O_3 substituted ferrites is more than that of pure one. In general, the density of substituted ferrites increases with the increase in As_2O_3 content, except for compositions with 2-3 mole percent of As_2O_3 and finally approaches a constant value. The increase in the density of substituted ferrites is due to the enhancement in the compactness of the material as a result of liquid phase sintering and the formation of solid solution resulting in the substitution of As^{3+} (At.wt = 74.92 amu) in place of some Fe^{3+} (At.wt. = 55.85 amu) lattice sites [39].

(iii) The decrease in the density of ferrites having compositions with 2-3 mole percent of As_2O_3 is compatible with the lattice parameter values determined. The increase in lattice parameters causes the increase in volume of the unit cell and consequently results in the decrease in the density.

(iv) With the increase in the sintering time and sintering temperature the density of all ferrite compositions

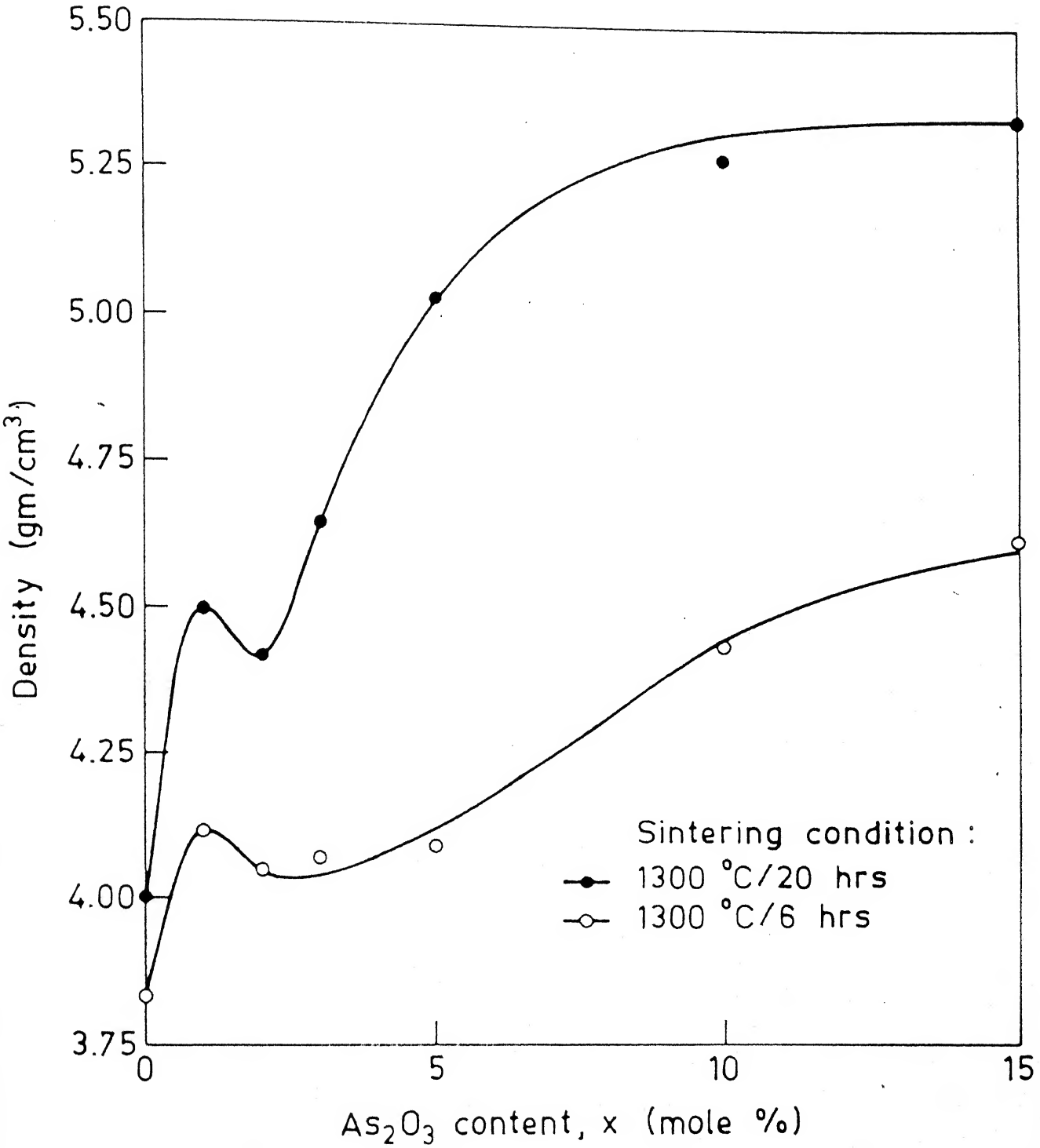

Fig. 3.2. Variation of density as a function of As_2O_3 content in Ba-ferrite.

increase due to increased ferritization and increased particle size.

3.3 X-RAY DIFFRACTION ANALYSIS

Standard ASTM X-ray diffraction data for $BaO.6Fe_2O_3$, α-Fe_2O_3 and As_2O_3 are given in Appendix B. The X-ray diffraction patterns for pure and As_2O_3 substituted ferrites sintered at 1300°C for 2 hrs have been shown in Fig. 3.3. Besides $BaO.6Fe_2O_3$ peaks, the asterik (*) marked peaks are due to α-Fe_2O_3 phase. The experimentally obtained X-ray diffraction data for pure (A0) and substituted (A3) ferrites are quoted in Tables 3.1 and 3.2 respectively. It is observed that in pure ferrite (A0), α-Fe_2O_3 peaks are present and the increase in As_2O_3 content causes decrease in intensity of α-Fe_2O_3 peaks and finally disappears for ferrite composition (A3). In addition to this, the substitution of As_2O_3 modifies the X-ray diffraction patterns (Fig. 3.3) of Ba-ferrite, i.e. it results in the shift of ferrite peaks through small angles and change in the half intensity line widths. Substitution of small amounts of As_2O_3 (mp $\sim$500°C) serves as catalyst to solid state reaction (ferritization) between BaO and Fe_2O_3 by providing liquid phase at the interface. Thus amount of ferrite formation increases initially with corresponding reduction in unreacted α-Fe_2O_3. A part of As_2O_3 also goes into solid solution (i.e., incorporates into the Ba-ferrite lattice) according to the

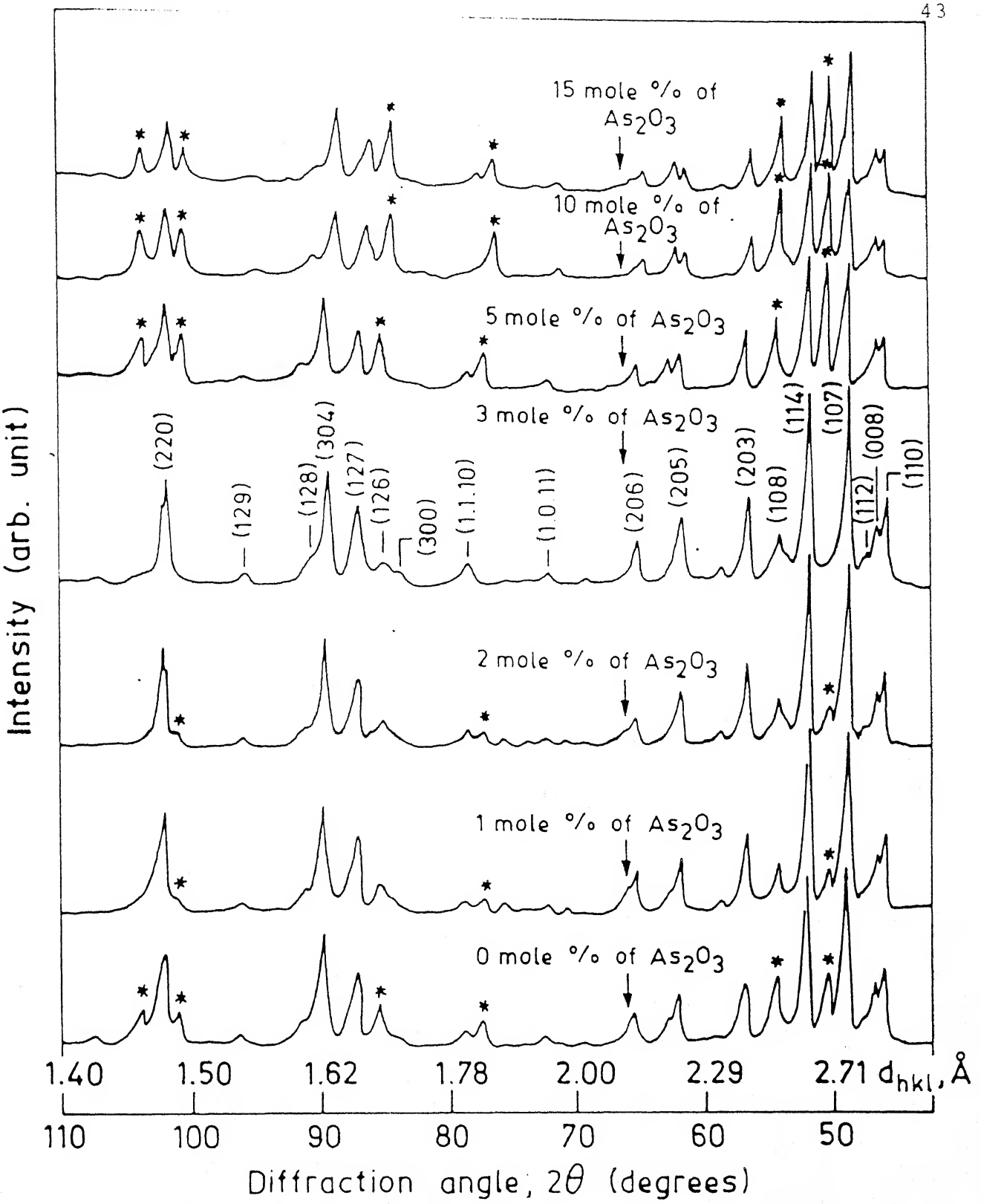

Fig. 3.3. X-ray diffraction (CrKα) patterns for pure and As_2O_3 substituted Ba-ferrite sintered at 1300 °C for 20 hours. Indexes (hkl) represents ferrite phase only. Fe_2O_3 peaks are asterik (*) marked.

Table 3.1

X-ray Diffraction (CrKα) Data for Pure Ba-Ferrite Composition AO Sintered at 1300°C for 20 hrs

2θ	d (A^{o})	Relative intensity I/I_1	(hkl)
45.88	2.938	38	(110)
46.36	2.910	20	(008)
47.40	2.85	15	(112)
48.78	2.774	100	(107)
50.34	2.693	40	(104)*
51.91	2.617	95	(114)
54.21	2.514	40	(108)
56.70	2.412	42	(203)
62.00	2.224	33	(205)
65.43	2.120	22	(206)
72.1	1.95	5	(1.0.11)
77.50	1.830	15	(0.24)*
78.3	1.814	11	(1.1.10)
83.9	1.713	5	(210)
85.41	1.689	22	(116)*
87.10	1.662	40	(126)
89.90	1.621	62	(127)
97.00	1.529	6	(304)
101.50	1.479	15	(128)
102.18	1.472	48	(129)
103.80	1.455	16	(220)

* - peaks correspond to α-Fe_2O_3 phase.

Table 3.2

X-ray Diffraction (CrKα) Data for Ba-Ferrite Composition A3 Sintered at 1300°C for 20 hrs

2θ (degrees)	d (A°)	Relative Intensity I/I_1	(hkl)
45.90	2.937	45	(110)
46.70	2.890	25	(008)
47.5	2.844	16	(112)
48.87	2.768	100	(107)
51.90	2.617	100	(114)
54.12	2.518	22	(108)
56.56	2.417	44	(203)
61.56	2.238	32	(205)
65.00	2.131	20	(206)
72.18	1.899	4	(1.0.11)
78.43	1.811	12	(1.1.10)
84.06	1.710	5	(210)
85.00	1.695	10	(126)
86.87	1.666	37	(127)
89.68	1.624	56	(304)
90.93	1.606	8	(128)
95.93	1.542	7	(129)
102.18	1.472	42	(220)

substitution $BaFe_{12-y}As_yO_{19}$ which is confirmed by the modified X-ray diffraction patterns [37] . However increasing amount of As_2O_3 beyond 5 mole percent, results in the precipitation of α-Fe_2O_3 owing to increasing amount of ionic substitution leading to increase in the intensity of α-Fe_2O_3.

The variation of half intensity line width ($\Delta 2\theta_{1/2}$) as a function of As_2O_3 content in Ba-ferrite for a particular peak (107) has been plotted in Fig. 3.4. The half line width depends upon two factors, the particle size (grain size) and the lattice strain (lattice distortion). Normally grain size of the material is 1μm or above. Thus the major effect of line broadening seems to be due to lattice strain. As is evident from Fig. 3.4, the line broadening passes through a maxima around 3 mole percent of As_2O_3 substitution. Thus it seems that the substitution of As_2O_3 strains the ferrite lattice to the maximum amount at this composition. It also corresponds to the maximum amount of incorporation of arsenic ion (As^{3+}) in the Ba-ferrite lattice.

The variation of lattice parameters, c&a, as a function of As_2O_3 content in Ba-ferrite has been shown in Fig. 3.5. At low concentrations of As_2O_3 ($\leq$ 2 mole %), both c&a are found to pass through local maxima. The value of lattice parameter, c, is minimum for the ferrite composition with 3 mole percent of As_2O_3 (A3). This composition also corresponds to maximum

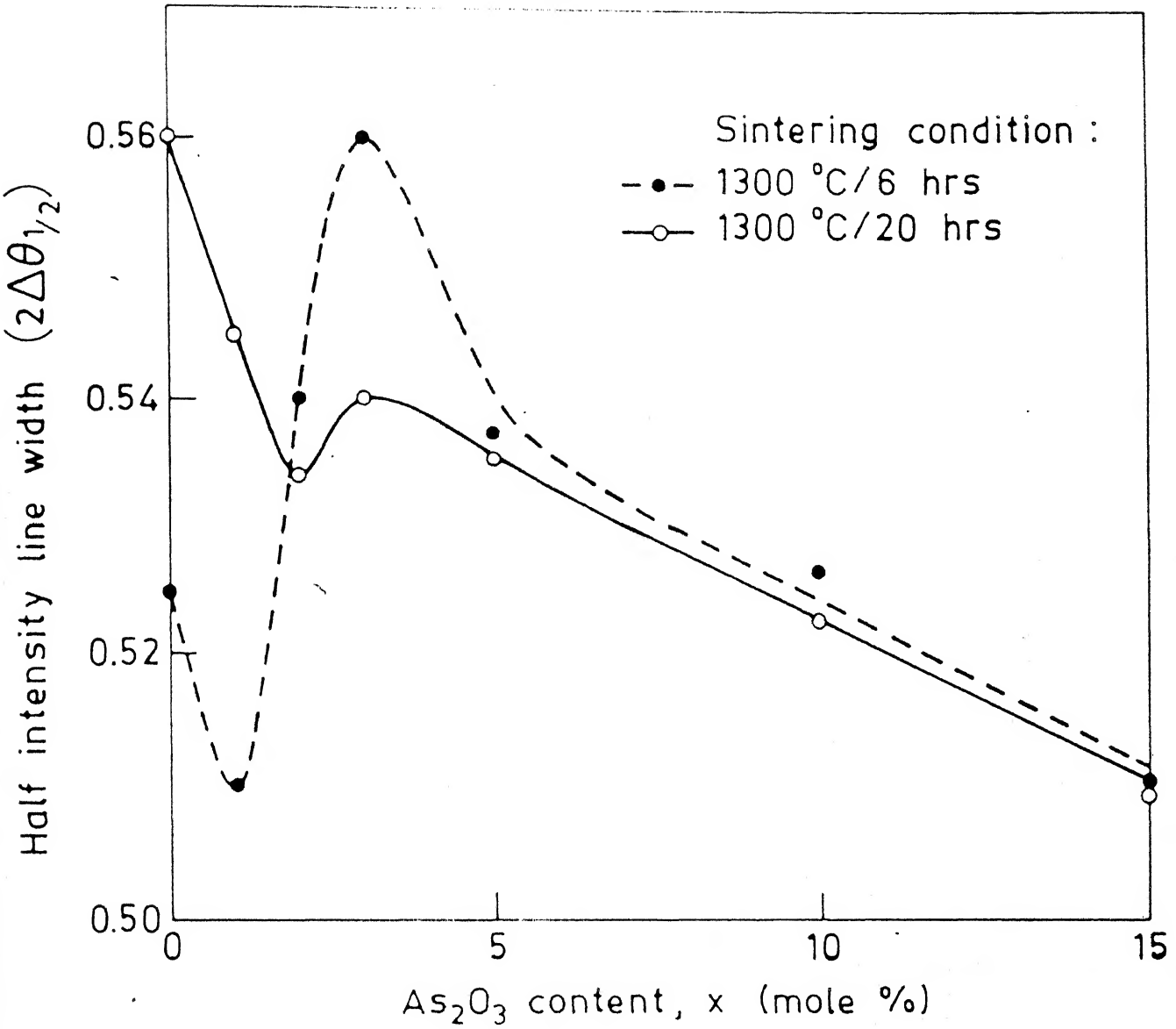

Fig. 3.4. Variation of X-ray diffraction line width for (107) line as a function of As_2O_3 content in Ba-ferrite.

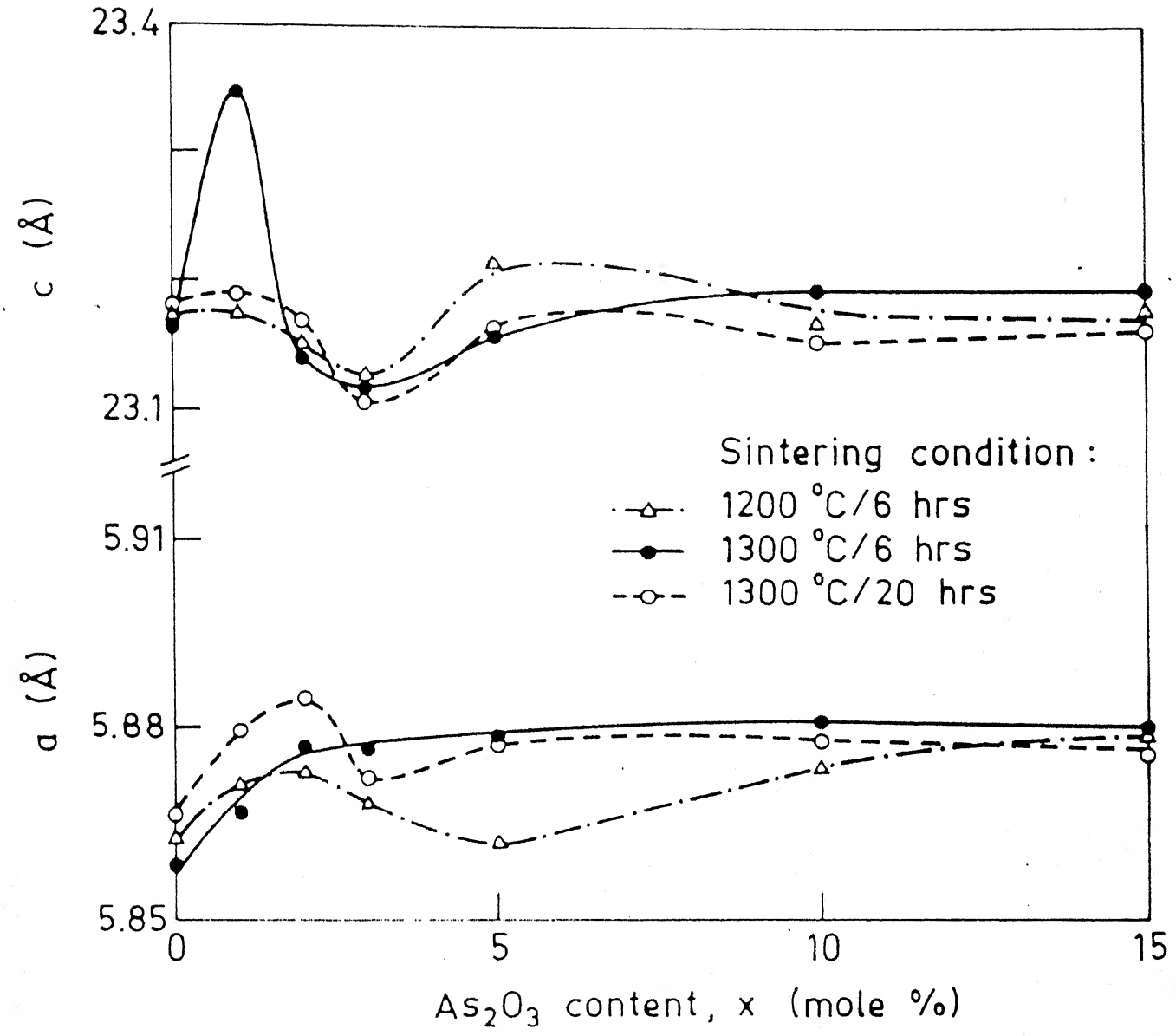

Fig. 3.5. Variation of Ba-ferrite lattice parameters, a & c as a function of As_2O_3 content.

distortion in the ferrite lattice.

3.4 ELECTRICAL MEASUREMENTS

3.4.1 Variation of Resistivity as a Function of Frequency

The variation of resistivity as a function of frequency at room temperature, for Ba-ferrites sintered at 1300°C for 20 hrs has been plotted in Fig. 3.6. The following salient features are observed:

(i) For frequencies below 10 KHz, the resistivity stays almost to a constant value depending upon the composition.

(ii) However beyond 10 KHz, the resistivity falls continously with increasing frequencies for all compositions.

(iii) A cross-over in the resistivity around 1.78×10^4 Ω-cm occurs at about 33 KHz.

(iv) After 33 KHz, the variation of $\log\rho$ is quite linear with log f. Also the resistivity of all the samples is of the same order at a given frequency.

(v) As the concentration of As_2O_3 increases, the resistivity decreases by approximately two orders of magnitude ($\sim 10^6$ Ω-cm to $\sim 10^4$ Ω-cm).

The variation of resistivity with frequency supports the applicability of the inhomogeneity model as given by Koops [24] for the polycrystalline ferrites. The decrease in resistivity with the increase in substitution could be attributed to the presence of As_2O_3.

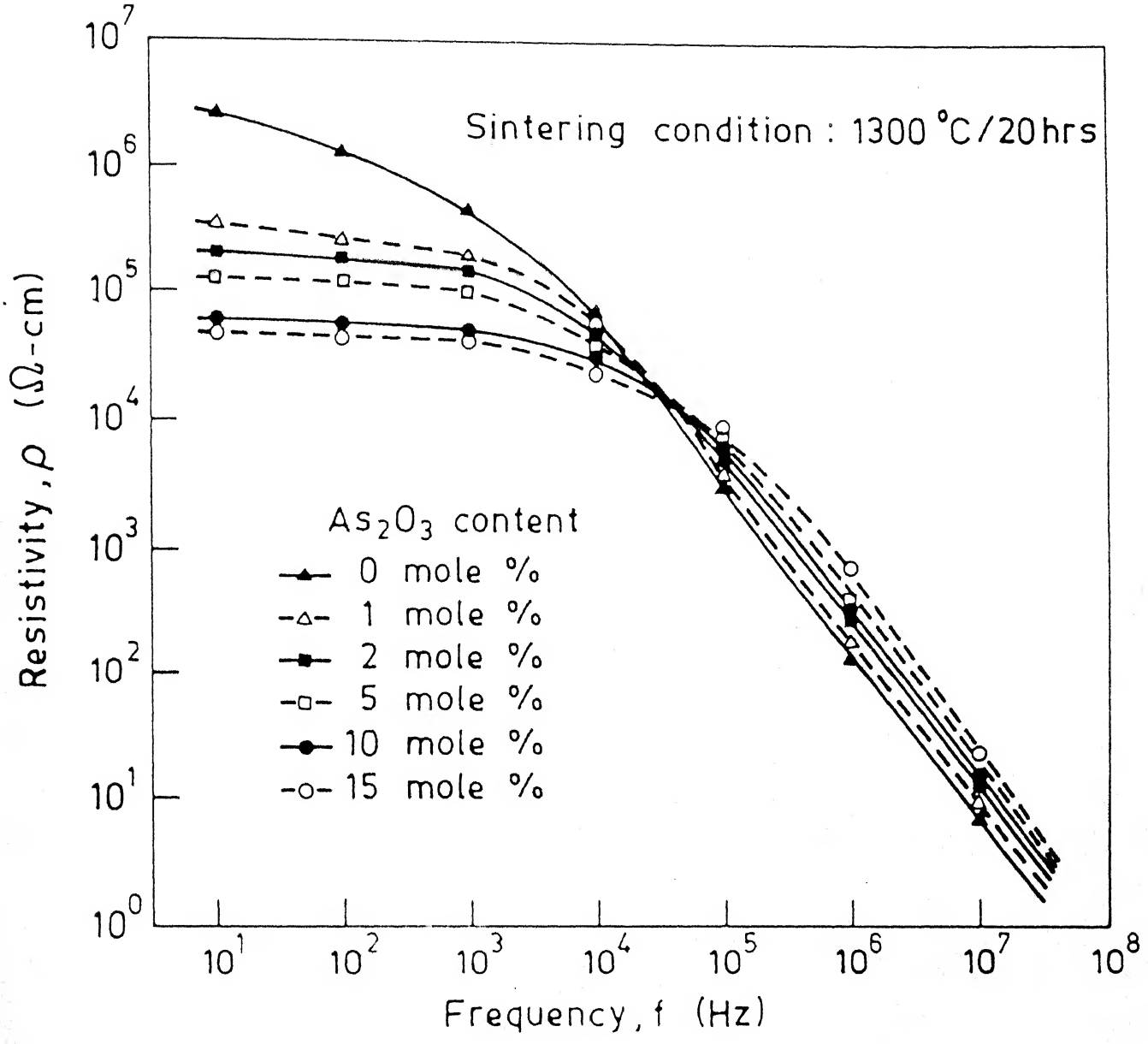

Fig. 3.6. Variation of resistivity with frequency for pure and As_2O_3 substituted Ba-ferrite sintered at 1300 °C for 20 hours.

3.4.2 Temperature Dependence of DC and AC Resistivity

(i) DC Resistivity

The variation of dc resistivity with temperature has been shown in Fig. 3.7 in terms of $\log\rho$ vs $10^3/T$ plot for pure ferrite (A0) and the As_2O_3 substituted ferrite (A1). The plot for both the compositions shows different activation energies for Region I (27^oC - 150^oC) and Region II (150^oC - 300^oC) as given in Table 3.3. Therefore there should be different dominating electrical conduction mechanisms for Region I and Region II. The activation energies for ferrite compositions A0 and A1 in Region I differ very little ($\sim$0.02 eV) from each other. This difference increases to $\sim$0.1 eV in Region II . In both the cases the activation energy for electrical conduction is lower for substituted Ba-ferrite (A1). This explains the decrease in resistivity with the substitution of As_2O_3 as observed. The conduction in the Region I seems to take place due to electron hopping mechanism between the exciting Fe^{3+} and Fe^{2+} ions [23] . The ionic conduction has been assumed to be absent. The high activation energy found at higher temperature may be accounted for by the creation of some more Fe^{2+} or Fe^{4+} ions under thermal activation.

(ii) AC Resistivity

The ac resistivity variation with temperature and frequency has been shown in Fig. 3.8. The results of pure ferrite (A0) and As_2O_3 substituted ferrite (A1) have been taken for

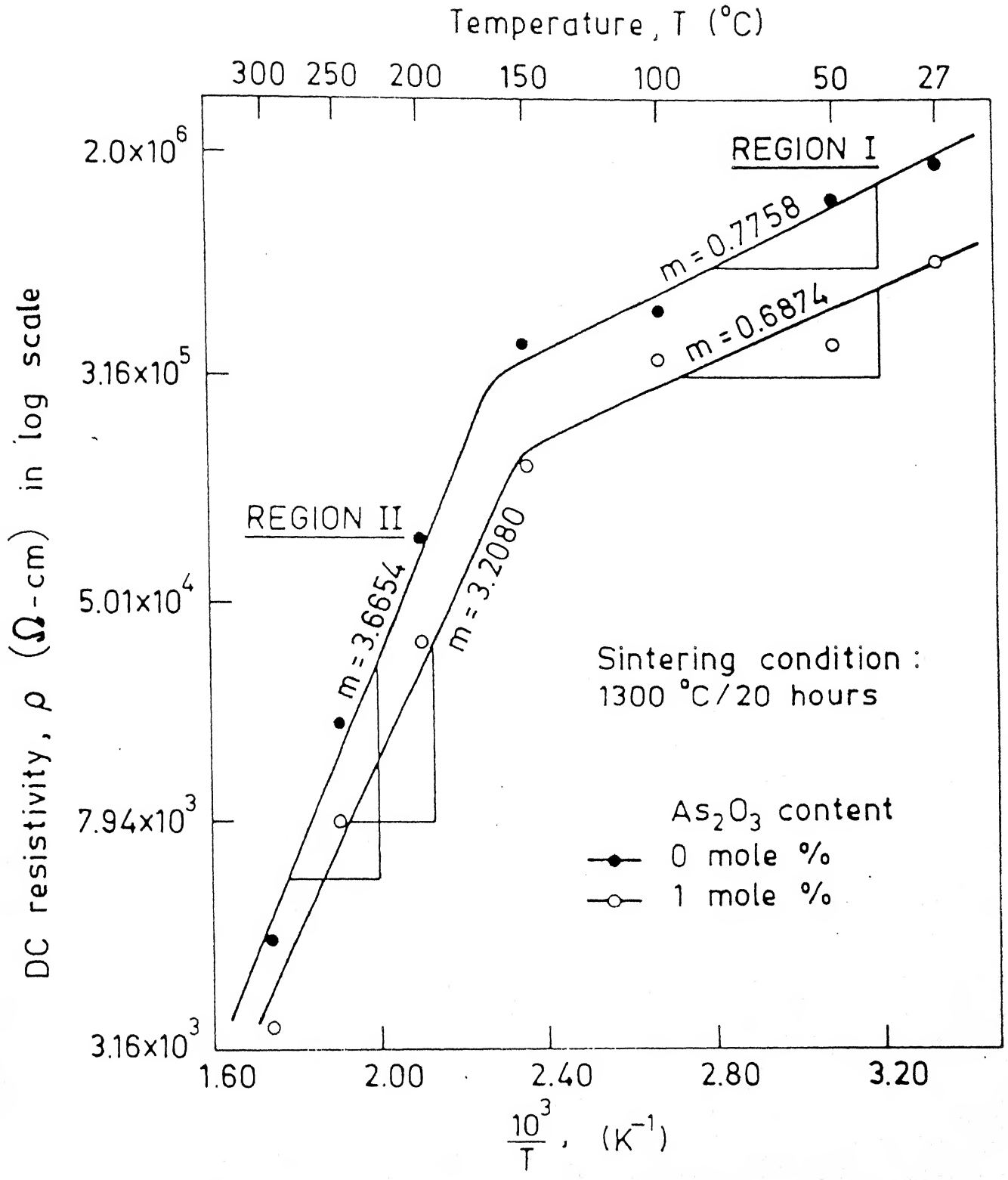

Fig. 3.7. Temperature dependence of DC resistivity for pure and As_2O_3 substituted Ba-ferrite sintered at 1300 °C for 20 hours.
('m' represents the slope)

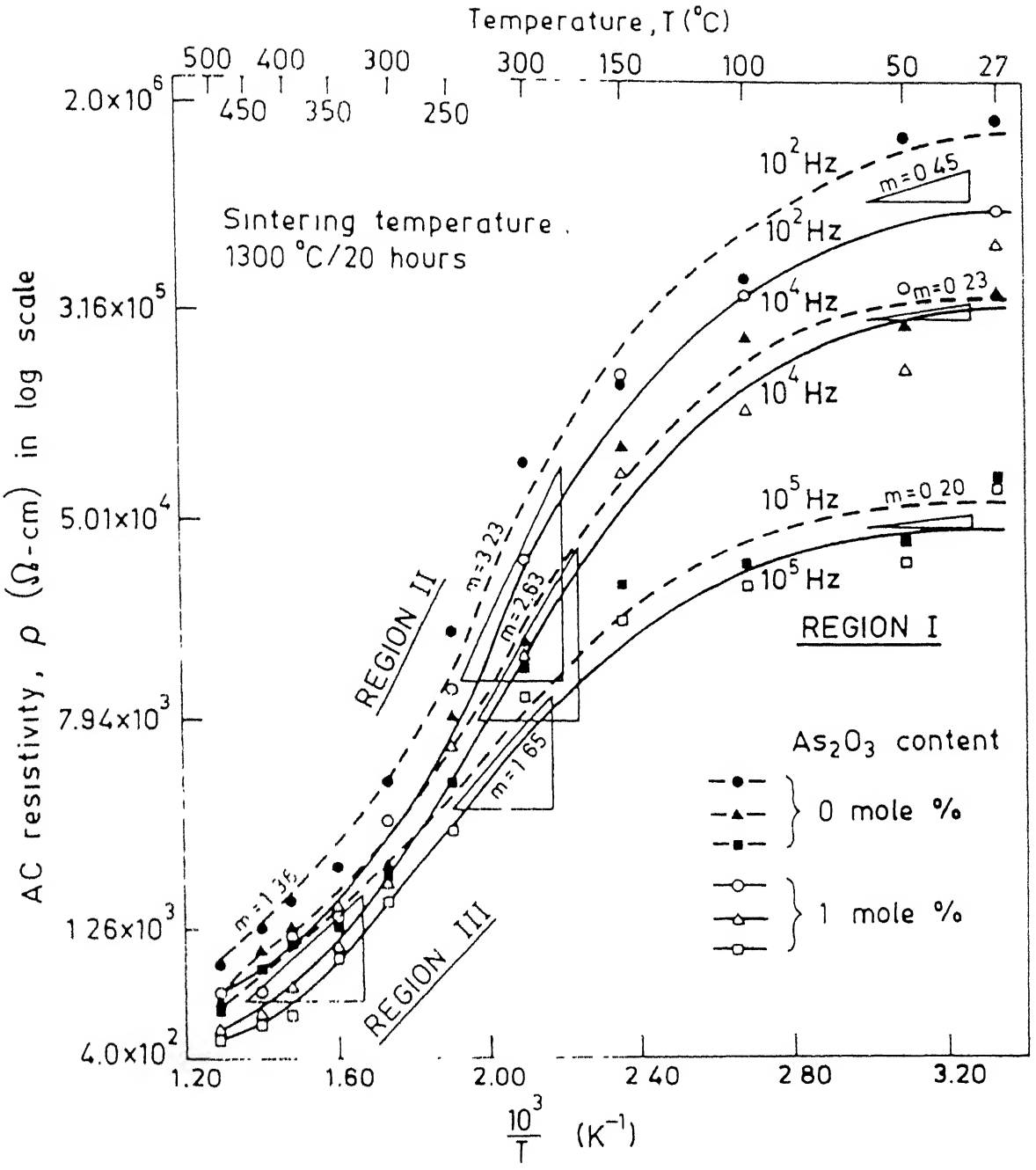

Fig. 3.8. Temperature dependence of AC resistivity at different frequencies for pure and As_2O_3 substituted Ba-ferrite samples sintered at 1300 °C for 20 hours.

Table 3.3

DC Activation Energies as Calculated from Fig. 3.7

Sample specification	Activation energy (Q) in eV	
	Region I ($27^{o}C$ - $150^{o}C$)	Region II ($150^{o}C$ - $300^{o}C$)
AO	0.154	0.728
A1	0.137	0.637

Table 3.4

AC Activation Energies at Different Frequencies as Calculated From Fig. 3.8

Frequency	Average of activation energies for ferrite compositions AO and A1 (Q) in eV		
	Region I ($27^{o}C$ - $150^{o}C$)	Region II ($150^{o}C$ - $300^{o}C$)	Region III ($300^{o}C$ - $500^{o}C$)
10^2	0.089	0.641	0.270
10^4	0.046	0.522	0.270
10^5	0.040	0.328	0.270

illustration. The resistivity is found to change continuously with temperature. It is seen that in Region III (300°C - 500°C), the resistivity values for both the compositions approaches each other at all the frequencies. The same differs appreciably from each other near room temperature at different frequencies. The values of activation energies at various frequencies and temperature ranges are given in Table 3.4. The following features are observed:

(i) The activation energy decreases with increasing frequency near room temperature and a relation of the type $Q \log f = C$, a constant, holds good.

(ii) The activation energy goes through a maximum in each case around 227°C. It is not clear what could be responsible for this behaviour. However, it can be argued that while electric conduction mechanisms in Region I (27°C - 150°C) and Region III (300°C - 500°C) are operating independently, the same in the intermediate temperature range (Region II) becomes sequential.

The general decrease in resistivity with increasing frequency is however in confirmity with the inhomogeneity model of ferrites [40].

3.4.3 Variation of Dielectric Properties as a Function of Frequency

The variation of dielectric constant ε' (real part of complex dielectric constant), dielectric loss ε'' (imaginary part

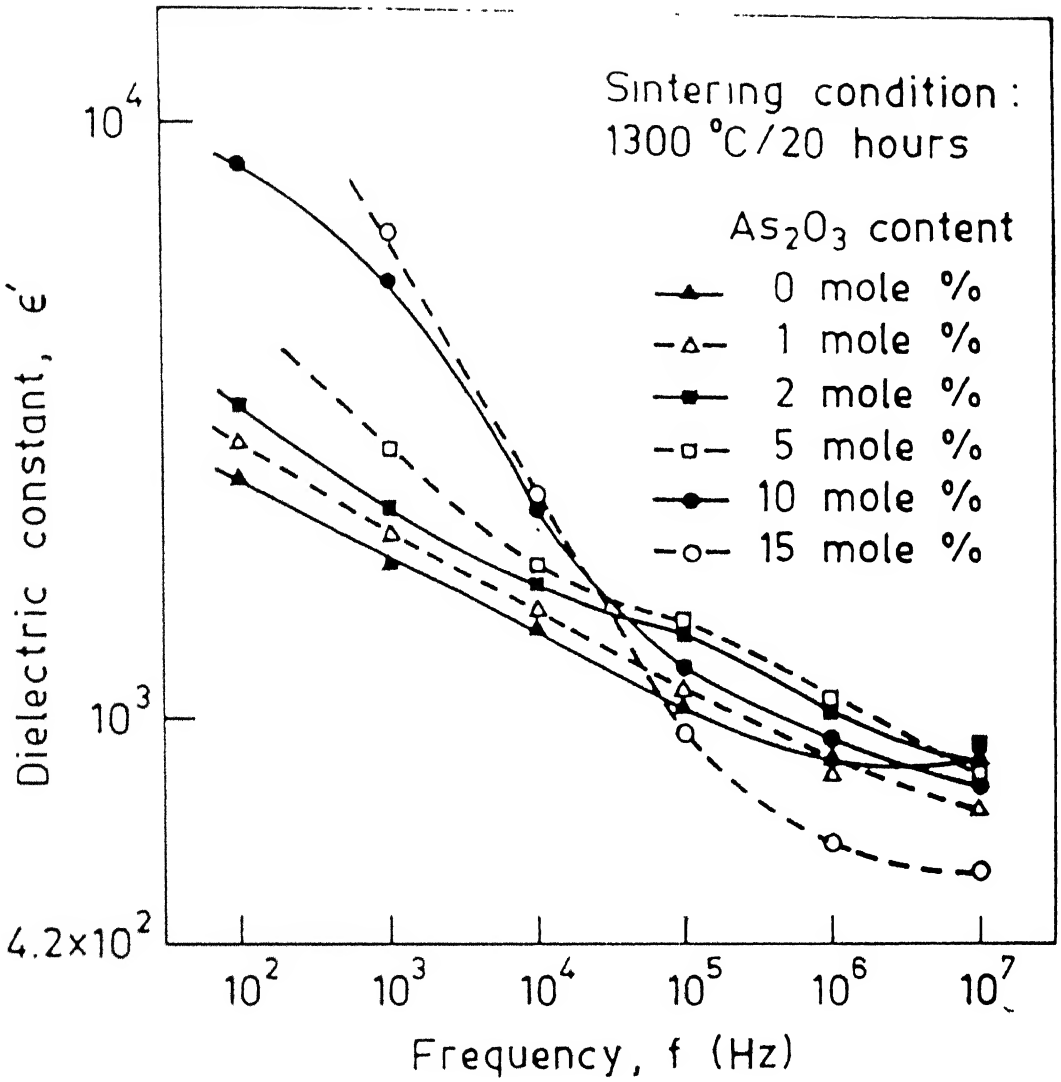

Fig. 3.9. Variation of dielectric constant with frequency for pure and As_2O_3 substituted Ba-ferrite sintered at 1300 °C for 20 hrs.

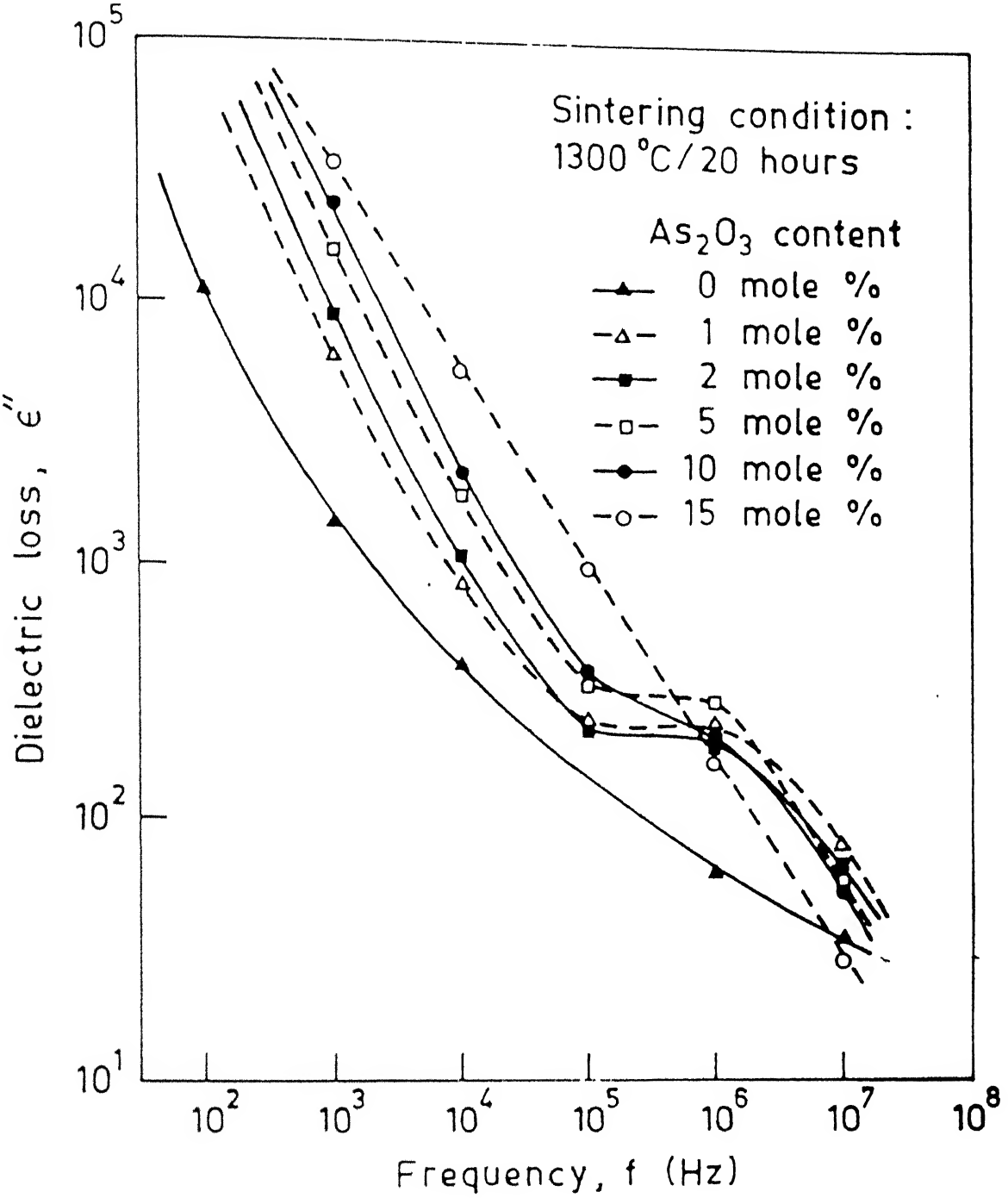

Fig. 3.10. Variation of dielectric loss with frequency for pure and As_2O_3 substituted Ba-ferrite sintered at 1300 °C for 20 hours.

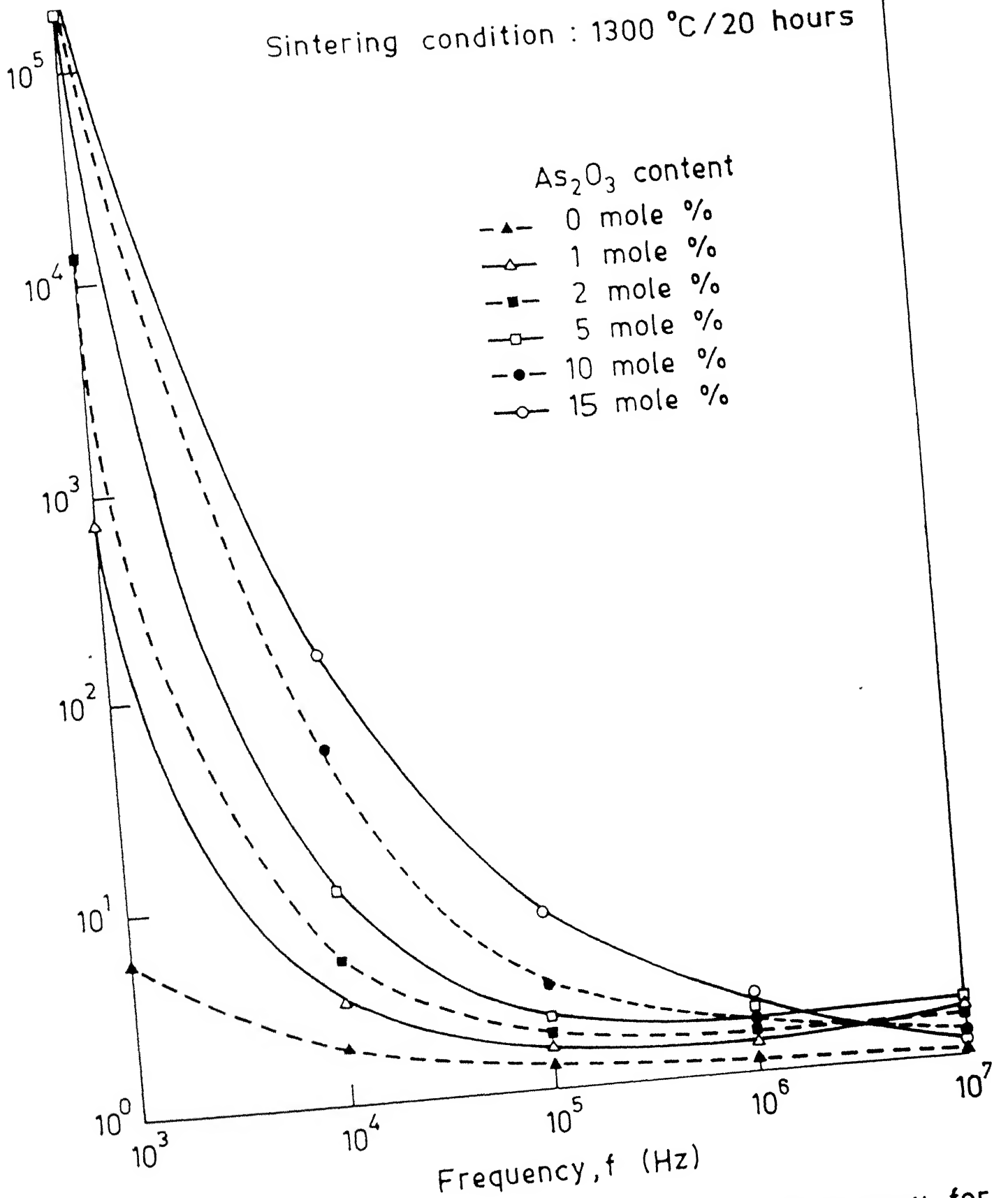

Fig. 3.11. Variation of dissipation factor with frequency for pure and As_2O_3 substituted Ba-ferrite sintered at 1300 °C for 20 hours.

complex dielectric constant) and dissipation factor (tanδ) as a function of frequency for Ba-ferrite sintered at 1300°C for 20 hrs has been shown in Figs. 3.9, 3.10 and 3.11 respectively. These figures exhibit following features:

(i) In general, the dielectric constant (ε'), dielectric loss (ε") and dissipation factor (tanδ) decrease with the increase in frequency. This behaviour may be explained on the basis of dielectric relaxation [40] in ferrites due to their structural inhomogeneity.

(ii) In general, the steepness (slope) of dielectric constant, dielectric loss and dissipation factor vs. frequency plots respectively is found to increase with increase of As_2O_3 content in ferrite. All these three quantities are found to increase, appreciably in the low frequency range, with the increase in As_2O_3 content in ferrite. This implies that As^{3+} impart enhanced polarisation effects to the ferrite lattice [8].

3.5 MAGNETIC MEASUREMENTS

The coercivity of Ba-ferrite compacts depends upon coercivity due to magnetocrystalline anisotropy, coercivity due to shape anistropy ($4\pi M_s$, for spherical particles) and particle size in general [17]. The specific saturation magnetization (σ_s) however depends upon composition, crystal structure and sintering temperature of ferrites. The

As_2O_3 substitution is thus expected to affect both of these properties as being discussed below.

3.5.1 Specific Saturation Magnetization

The variation of specific saturation magnetisation with increasing amount of As_2O_3 content has been shown in Fig. 3.12. Following three features are evident:

(i) The specific saturation magnetisation decreases continuously with increasing amount of As_2O_3 content beyond 5 mole percent. This may be attributed to dilution of magnetic ions (Fe^{3+}) per unit mass of the ferrite compact.

(ii) In the 0-5 mole percent range of As_2O_3 content, the specific saturation magnetisation of ferrites passes through a maximum or minimum around 1 mole percent of As_2O_3 content. The continuously increasing or decreasing value of σ_s with As_2O_3 content in this range can be attributed to the incorporation of nonmagnetic ion (As^{3+}) in place of magnetic ion (Fe^{3+}) in the ferrite lattice. If the replaced magnetic ion (Fe^{3+}) has the magnetic moment parallel to the net magnetic moment of lattice, the σ_s will decrease, otherwise σ_s will increase [41,42].

(iii) While the slope of σ_s vs. As_2O_3 content is nearly identical for different types of processed materials having composition with 5-15 mole percent of As_2O_3. It varies differen tly for materials having composition with 0-5 mole percent of As_2O_3 with different processing history.

This composition range is therefore very interesting from materials processing point of view.

3.5.2 Coercivity

The variation of coercivity with As_2O_3 content has been shown in Fig. 3.13. It is interesting to note that this variation passes through a maximum at about 1-2 mole percent of As_2O_3 and a minimum at about 3 mole percent of As_2O_3. This behaviour is found to be parallel to the variation of lattice parameter, c, as shown in Fig. 3.5. The origin of this behaviour can therefore be attributed to change in lattice parameter, c, and the associated magneto-crystalline energy with it. Thus larger the value of lattice parameter, c, higher will be the coercivity value and vice versa. Here we have assumed that the effect of particle size on the H_c is negligible for all the compositions synthesised at a particular sintering condition. It should be noted that the H_c ($\geq$ 3 KOe) usually observed in the Ba-ferrites containing no additive species is too large to be of much use in magnetic recording applications [43].

It has also been observed that with increasing the sintering time and sintering temperature, in general, the coercivity decreases. It is due to increase in particle size resulting in the increase in the formation of multidomain ferrite particles [44,45].

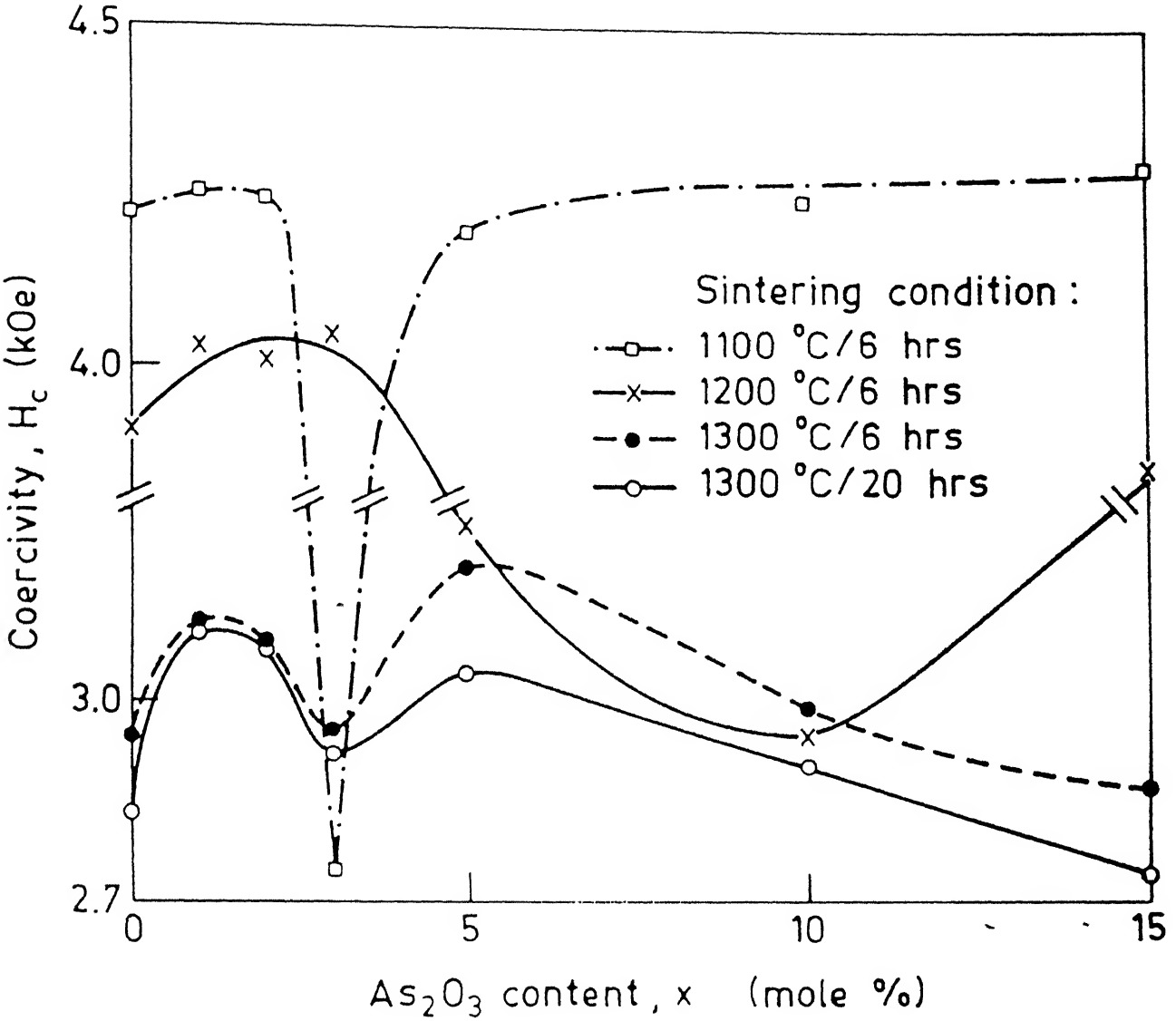

Fig. 3.13. Variation of coercivity as a function of As_2O_3 content in Ba-ferrite.

CHAPTER 4

CONCLUSION

The conclusions based on the observations made using following experimental techniques are as follows:

1. Optical Microscopy:

(i) The optical micrographs reveal that the substitution of As_2O_3 in the Ba-ferrite ($BaO.6Fe_2O_3$) enhances the liquid phase sintering thereby increasing the ferritization at a given sintering condition as compared to that of pure Ba-ferrite.

(ii) Particle size is found to increase for As_2O_3 content 0-3 mole percent.

(iii) It also reveals that the ferrite particles disperse more homogeneously throughout the material on increasing the As_2O_3 content.

2. Density Measurements:

(i) The density of Ba-ferrite increases with the increase in As_2O_3 content, except for ferrite composition with 2 mole percent of As_2O_3 (A2), and finally approaches a constant value for 15 mole percent of As_2O_3 content.

(ii) The density of a given composition increases with increasing sintering temperature and sintering time.

3. X-ray Diffraction Analysis:

(i) The ferrite formation increases with the increase in As_2O_3 content till 3 mole percent and at this composition ferritization is almost complete. Beyond 3 mole percent of As_2O_3 content ferritization is found to decrease.

(ii) The substitution of As_2O_3 in Ba-ferrite modifies the X-ray diffraction patterns, thereby confirming that a part of As_2O_3 dissolves into the Ba-ferrite lattice according to substitution $BaFe_{12-y}As_yO_{19}$.

(iii) The formation of solid solution with the substitution of As_2O_3 in Ba-ferrite strains the lattice and it is maximum for the composition A3. It results in the change in lattice parameters, a and c.

4. Electrical Measurements:

(i) The dc resistivity of the pure Ba-ferrite is $\sim 10^6$ Ω-cm and it is found to decrease with the substitution of As_2O_3 in the Ba-ferrite.

(ii) The resistivity at a given frequency is found to decrease with increasing As_2O_3 content in Ba-ferrite in the

frequency range 10^1 - 10^4 Hz and beyond 10^4 Hz the resistivity decreases rapidly for all the compositions. At 10^7 Hz, the resistivity is $\sim$10 Ω-cm for all compositions.

(iii) The dc activation energy for pure ferrite in the temperature range 27°C - 150°C is $\sim$0.15 eV and in the temperature range 150°C - 300°C is $\sim$0.7 eV. With the substitution of As_2O_3, the activation energy decreases in both the temperature range.

(iv) The ac activation energy is found to decrease with the increase in the frequency applied.

(v) With increasing the substitution of As_2O_3, the dielectric constant (ε') the dielectric loss (ε'') and the dissipation factor ($\tan\delta$) increase. Also these parameters decrease rapidly with the increase in frequency applied for all the compositions synthesised.

5. Magnetic Measurements:

(i) The variation of specific saturation magnetisation (σ_s) as a function of As_2O_3 content shows complex behaviour (Fig. 3.12). For the ferrite compositions sintered at different sintering conditions, except that sintered at 1300°C for 20 hrs, the σ_s is found to decrease with increase in As_2O_3 content in Ba-ferrite with few maxima and minima.

(ii) The coercivity (H_c) initially increases with the increasing As_2O_3 content upto 1-2 mole percent. For the composition with 3 mole percent of As_2O_3 (A3), the H_c falls abruptly. H_c values again increase. The coercivity decreases with increasing sintering time and sintering temperature.

REFERENCES

1. H. Kojima, Ferromagnetic Materials, Vol. 3, ed. E.P. Wohlfarth, North-Holland Publishing Company, 1982.

2. E.S. Borovik and N.G. Yakovleva, Fiz. Metal. Metalloved, 13 (1962a), 470.

3. E.S. Borovik and N.G. Yakovleva, Fiz. Metal. Metalloved., 15 (1963), 511.

4. K. Haneda and H. Kojima, Phys. Status. Solidi, A6 (1971) 259.

5. K. Haneda and H. Kojima, Japan J. Appl. Phys., 12 (1973b), 355.

6. T.M. Perekalina and V.P. Cheparin, Fiz. Tverd. Tela, 9 (1967) 217.

7. A.P. Kirichok, N.B. Voroninia, O.F. Verezhok and V. Ya. Garmash, "Effect of Additions of Praseodymium and Bismuth Oxides on the Properties of Barium Hexaferrites", Soviet Powder Metallurgy and Metal Ceramics, 24, 3 (267), (1985), p. 229.

8. H. Krishnan, M.Tech. Thesis, Materials Science, I.I.T., Kanpur, May 1987.

9. N.K. Ghosh, M.Tech. Thesis, Met. Engg., I.I.T.,Kanpur, 1981.

10. N.K. Ghosh, A.R. Das and K.N. Rai, "Preparation, Characterisation and Magnetic Property of Coprecipitated Barium Hexaferrite Powders", Trans. Indian Cera. Soci., 43(4) (1984), 89.

11. T.M. Oran, "Ba-ferrites Hot Pressing Process for Preparing High Quality Material from very Fine Powders", IEEE Trans. Mag., Sept. (1975), 1452.

12. J.M. Desvigues, H. Lee Gall, M. Laberyie, J.C. Mage, Cobinsion, "Improvement of Hexaferrites, Crystal Growth Reproductibility and Characterisation", Journal De Physique, 46 (1985), 326.

13. A.M. Morisicko, Matsurroto and Minaoe, "C-axis Orientation of Hexagonal Films Prepared by R.F. Sputtering", IEEE Trans. Magnetics, 5PG4, 1981-82.

14. K.J. Standley, "Oxide Magnetic Materials", Monographs on the Physics and Chemistry of Materials, 1962.

15. P. Krishna, "Characterisation of Polytype Structures", 1976.

16. P.B. Braun, Philips Res. Rep., 12 (1957), 491.

17. B.D. Culity, Introduction to Magnetic Materials, Wesley Publishing Company, 1972.

18. F.G. Brakman, "Magnetic Ceramics", A Review and Status Report, American Ceramic Society Bulletin, 47(1), Feb. (1968) 186.

19. D. Hadfield, Permanent Magnets and Magnetism, London ILIFFE Books Ltd. (1962).

20. Cleveland, "Magnetic Properties of Metals and Alloys", American Society of Metals, 1954,
(a) p.146, (b) p. 151, (c) p. 152.

21. R.M. Bozorth, Ferromagnetism, N.Y., Van Nostrand, 1959.

22. S. Chikazumi, Physics of Magnetism, N.Y., J.Wiley, 1964.

23. K. Zaveta, Phys. Status Solidi, 3 (1963) 2111.

24. C.G. Koops,"Dispersion of Resistivity and Dielectric Constant of Some Semiconductors at Audio Frequency", Phys. Rev., 83 (1951) 121.

25. J.J. Went, G.W. Rathenau, E.W. Gorter and G.W. Van Osterhout, Phil. Techn. Rev., 13 (1952) 194.

26. J. Smit and H.P.J. Wijn, Ferrite, Philips Tech. Bibl., Hamburg (1962).

27. K. Haneda, C. Mivakawa and H. Kojima, J. Amer. Ceramic Soc., 57 (1974a) 354.

28. K. Haneda and H. Kojima, J. Appl. Phys., 44 (1973a), 3760.

29. J.J. Becker, Metallurg. Rev., 7 (28) (1962) 371.

30. N.J. Cliffs, Theory and Application of Ferrites, Princeton Hall, 1960.

31. H.J. Caspar and G. Samow, Valvo. Ber., 11 (1965), 136.

32. A. Passerone, E. Biagini and V. Lorenzelli, Ceramurgia Int., 1 (1) (1975), 23.

33. H. Stablein, Ferromagnetic Materials, Vol. 3, ed. E.P. Wohlfarth, North-Holland Publishing Company, 1982.

34. J. Bereketa and M.J. Ridge, "The Reaction between Iron (III) Oxide and $BaCO_3$ in Vacuum", J. of Chem. Soc., (1968), 2463.

35. E.C. Snelling, "Properties of Ferrites in Relation to their Applications", Proc. Br. Ceramic Soc., 2 (1964),151.

36. R. Grossinger, Phys. Stat. Sol., (a) 66 (1981), 665.

37. S. Ram, D. Bahadur and D. Chakravorty, "Magnetic Properties of $BaFe_{12}O_{19}$ Particles with B_2O_3 Addition", Journal of Mag. and Mag. Matls., North-Holland, Amsterdam, 71 (1988) 359.

38. J. Smit and H.P.J. Wijin, Ferrites, Philips Techn.Lib., Eindhoven, (1959), 177.

39. F. Bradley, Materials for Magnetic Functions, Hyden Book Company, Inc., New York.

40. F. Haberey and H.P.J. Wijn, "Effect of Temperature on the Dielectric Relaxation in Polycrystalline Ferrites", Phys. Stat. Sol., 26 (1968), 26.

41. G. Bate, Ferromagnetic Materials, Vol. 2, ed.E.P.Wohlfarth, North-Holland, Amsterdam, 1982.

42. A. Collomb, P. Wolfers and X. Obradors, J. Magn. Magn. Mat., 62 (1986), 57.

43. T. Fujiwara, IEEE Trans. Magn. MAG-21, (1985), 1480.

44. M. Vallet, P. Rodriguez, X. Obradors, A. Isalgue, J. Rodriguez and M. Pernet, J. de Phys., 46 (1985), C6-335.

45. O. Kubo, T. Ido, H. Yokoyama and Y. Koike, J. Appl. Phys., 57 (1985), 4280.

APPENDIX A

IONIC RADII OF SEVERAL IONS

Table A1

Ionic Radii of Several Ions (Pauling 1960)

Element	Valence	Radius (A^{o})
Ag	+1	1.26
Al	+3	0.50
As	+3	0.58
Ba	+2	1.35
Bi	+3	0.96
Cr	+3	0.63
Fe	+2	0.74
	+3	0.64
Ga	+3	0.62
In	+3	0.81
La	+3	1.15
Na	+1	0.95
O	-1	1.40
P	+3	0.44
Pb	+2	1.20
Sc	+3	0.81
Sr	+2	1.13
Zn	+2	0.74

APPENDIX B

DIELECTRIC BEHAVIOUR OF POLYCRYSTALLINE FERRITES

Dielectric behaviour of polycrystalline ferrites was explained by Koops [1]* on the basis of Maxwell-Wagner layer model for inhomogeneous dielectric (Fig. B.1). Koops assumed that both the grains and boundaries can be represented by parallel R-C circuits. A series combination of these parallel circuits would then represent the behaviour of inhomogeneous dielectric as a whole. This is shown in Fig.B.

C_p and R_p are the equivalent parallel capacitance and equivalent parallel resistance respectively as shown in Fig.B.3. Therefore the admittance Y_p of the circuit shown in Fig. B.2 is

$$Y_p = \frac{1}{R_p} + j\omega_p \qquad (B.1)$$

where

$$R_p = \rho_p \frac{L}{A}$$

$$C_p = \varepsilon_o \varepsilon_p \frac{A}{L}$$

where ρ_p and ε_p are the resistivity and dielectric constant of the ferrite respectively. A is cross-sectional area of the specimen; L is the length between two electrodes.

---

* C.G. Koops, Phys. Rev., 83 (1951) 121.

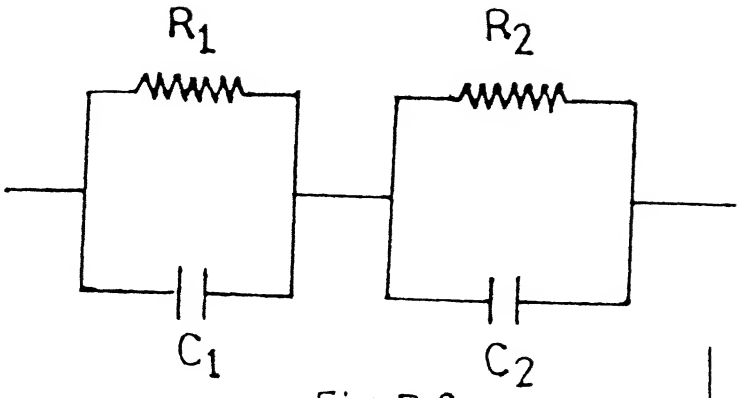

Fig. B 2

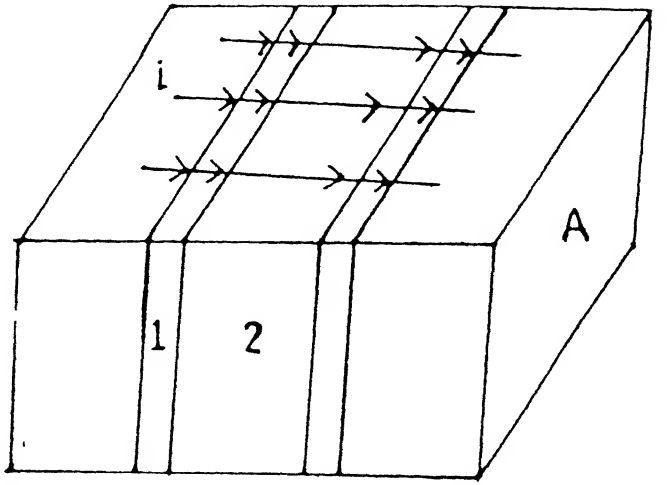

Fig.B 1 Inhomogenous Dielectric Structure

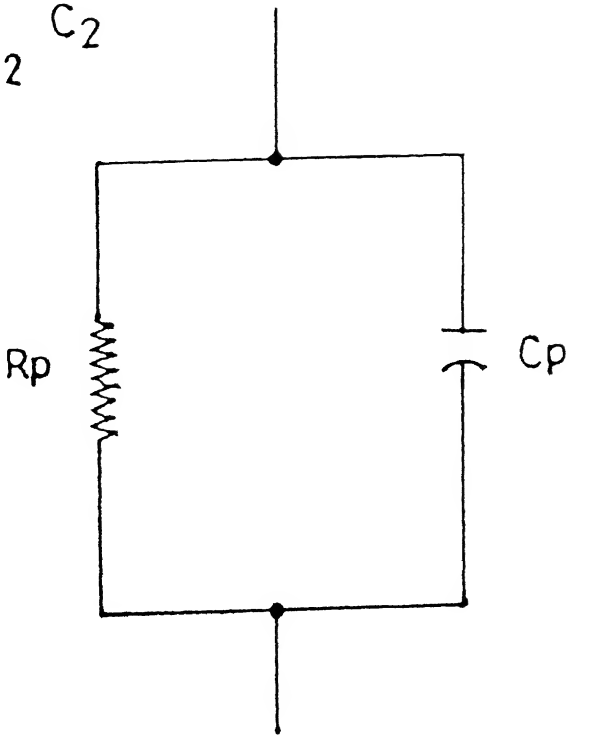

Fig.B 3. Equivalent Circuit of Ferrite Dielectric

Fig.B Polycrystalline Structure of Ferrites - Dielectric Structure.

When A.C. field is applied on dielectric material which does not have free charges, this causes periodic polarization. However polarized charge, lag behind applied A.C. field. Under such circumstances losses in the capacitor are represented by a complex dielectric constant

$$\varepsilon = \varepsilon_p' - j\,\varepsilon_p'' \qquad \text{(B.2)}$$

where ε_p' is real part of complex dielectric constant, ε_p'' is imaginary part of complex dielectric constant under experimental conditions. R_p is quite large and thus admittance is

$$Y_p = j\omega C_p = j\omega\varepsilon_o \frac{A}{L} \qquad \text{(B.3)}$$

$$\therefore \quad Y_p = j\omega\,\varepsilon_o \frac{A}{L}\,\varepsilon_p' - j\varepsilon_p'' \qquad \text{(B.4)}$$

Equating equations (B.1) with (B.4) we have

$$\frac{1}{R_p} + j\omega C_p = j\omega\,\varepsilon_o \frac{A}{L}(\varepsilon_p' - j\varepsilon_p'') \qquad \text{(B.5)}$$

Comparing real and imaginary parts on both sides

$$\varepsilon_p'' = \frac{L}{\omega\,\varepsilon_o\,A\,R_p} = \frac{1}{\omega\varepsilon_o} = \frac{\sigma}{\omega\varepsilon_o} \qquad \text{(B.6)}$$

It is imaginary component of complex dielectric constant, but it is real, usually called as dielectric loss,

$$\therefore \text{ Dielectric loss } (\varepsilon_p'') = \frac{\sigma}{\omega \varepsilon_o}$$

and

$$\varepsilon_p' = C_p \times \frac{1}{A\varepsilon_o} \tag{B.7}$$

It is a real component, known as dielectric constant. In the phase diagram δ is the phase angle between ε_p' and ε_p''. The tanδ (loss tangent), is the measure of dissipcation and it can be expressed as

$$\tan = \varepsilon_p'' / \varepsilon_p' \tag{B.8}$$

After combining equations (B.2) to (B.6) it leads to

$$\tan = \frac{1}{\omega C_p R_p} = \frac{\varepsilon_p''}{\varepsilon_p'} = \frac{1}{\omega \varepsilon_o \varepsilon_p} \tag{B.9}$$

Since loss tagent (tanδ) can be taken as D (dissipation factor) directly from admittance bridge. Then quality factor of the ferrite can be given by:

$$Q = \frac{1}{\tan\delta} = \frac{1}{D} = \omega C_p R_p \tag{B.10}$$

Quality factor tells about how much energy is dissipated in one complete cycle.

Determining the admittance using electric circuit from Fig. (B.2) and equating with equation (B.1) with following assumptions:

$$x = d_1/d_2 \ll 1$$

$$\rho_1 \gg \rho_2$$

$$\rho_1 > \rho_2$$

$x\rho_1 > \rho_2$ by a reasonable factor

$$\varepsilon_1 = \varepsilon_2$$

where d_1 = grain boundary thickness

d_2 = grain size

$x = (\frac{d_1}{d_2})$ is the ratio of thickness of the grain boundary layer to the thickness of crystallites.

Koops arrived at

$$\rho_p = \rho_2 + \frac{x\rho_1}{1 + \frac{C'\rho_1 \rho_2 \omega^2}{x}} \qquad (B.11)$$

where,

ρ_1 and ρ_2 are resistivity of layers which are marked (1) and (2) in Fig. B.1

$$\varepsilon_p = C_2 + \frac{\varepsilon_2/x}{1 + \frac{C' \rho_2^2 \omega^2}{x^2}} \qquad (B.12)$$

The equations (B.11) and (B.12) tell low resistivity and electric constant relaxation with applied frequency.

If the relevant dimension 'd' of a ferrite sample is larger than half as the wavelength inside the ferrite medium, standing waves are set up which give rise to high magnetic and dielectric losses. This phenomenon is known as dimensional resonance. Thus dimensional resonance occurs if

$$d > \frac{\lambda_m}{2} = \frac{c}{2f} \cdot \frac{1}{\sqrt{\mu_r \varepsilon_p / \varepsilon_o}} \qquad (B.13)$$

where λ_m = wave length and μ_r = relative permeability.

At low frequencies when relative permeability μ_r and $\varepsilon_p/\varepsilon_o$ are both high, dimensional resonance may occur in a ferrite of ordinary dimensions.

So summarizing the relaxation effects, we have from equations (B.11) and (B.12):

when $f \to 0$ $\rho_p \to x\rho_1$

(low frequency) and $\varepsilon_p \to \varepsilon_1/x$

when $f \to \infty$ $\rho_p \to \rho_2$

(high frequency) and $\varepsilon_p \to \varepsilon_2$

At low frequencies the impedance of the crystallite is negligible as compared to the boundary. At high frequencies the boundary capacitance short circuits the boundary resistance and bulk dielectric properties approach that of the crystallite.

APPENDIX C

X-RAY DIFFRACTION DATA FOR SOME COMPOUNDS

Table C1

X-ray Diffraction Data for $BaO.6Fe_2O_3$ (ASTM File No. 7-276)

$2\theta^{\dagger}$ (degrees)	d (A^{o})	Relative Intensity I/I_1	(hkl)
45.86	2.94	40	(110)
46.70	2.89	13	(008)
47.39	2.85	10	(112)
48.85	2.77	100	(107)
51.85	2.62	100	(114)
54.07	2.52	8	(108)
56.50	2.42	40	(203)
61.81	2.23	40	(205)
65.06	2.13	25	(206)
72.16	1.945	10	(1.0.11)
78.31	1.814	16	(1.1.10)
83.81	1.715	6	(210)
84.79	1.699	10	(126)
86.88	1.666	40	(127)
89.65	1.625	50	(304)
91.00	1.606	6	(128)
96.95	1.530	10	(129)
102.09	1.473	40	(220)

† Calculated for

Table C2

X-ray Diffraction Data α-Fe_2O_3 (ASTM File No. 13-534)

$2\theta^{\dagger}$ (degrees)	d (A°)	Relative Intensity I/I_1	(hkl)
50.40	2.69	100	(104)
54.30	2.51	50	(110)
62.72	2.201	30	(113)
77.10	1.838	40	(024)
85.34	1.690	60	(116)
91.73	1.596	16	(018)
101.73	1.484	35	(214)
104.16	1.452	35	(300)

+ Calculated for CrKα radiation, $\lambda = 2.291002\ A^{\circ}$.

Table C3

X-ray Diffraction Data for As_2O_3 (ASTM File No. 4-566)

$2\theta^{\dagger}$ (degrees)	d (A°)	Relative Intensity I/I_1	(hkl)
42.01	3.195	100	(222)
48.89	2.768	28	(400)
53.59	2.541	38	(331)
60.85	2.262	12	(422)
64.10	2.132	17	(511)
71.65	1.957	27	(440)
75.4	1.873	6	(531)
76.7	1.846	5	(600)
86.62	1.670	21	(622)
91.51	1.599	10	(444)
95.22	1.551	22	(711)

† Calculated for CrKα radiation, λ = 2.291002 A°.

APPENDIX D

Table D1

Properties of Barium Hexa-Ferrite at Room Temperature

S.No.	Property		Value	References*
1.	**STRUCTURAL PROPERTIES**			
	i) Lattice constants,	a	5.89 A^{o}	1
		c	23.20 A^{o}	
	ii) Thermal expansion coefficients,	α_a	$18.6 \times 10^{-6}/^{o}K$	2
		α_c	$17.2 \times 10^{-6}/^{o}K$	
	iii) Density (X-ray)		5.29 gm/cm^3	1
2.	**ELECTRICAL PROPERTIES**			
	i) D.C. resistivity		$\sim 10^{6}\ \Omega$-cm	3
	ii) Dielectric constant, (ε'), at 30 Hz		$\sim 2.5 \times 10^{3}$	4
	at 10^{5} Hz		$\sim 1.2 \times 10^{3}$	
3.	**MAGNETIC PROPERTIES**			
	i) Saturation magnetization, M_s		3800 gauss	5
	or specific saturation magnetization; σ_s		70.7 emu/gm	
	ii) Remanent magnetization, M_r		2050 gauss	
	or remanent specific magnetization, σ_r		35 emu/gm	
	iii) Coercive field, H_c		2400, Oe	
	iv) Maximum energy product $(BH)_{max}$		0.85 K Gauss.Oe	

Contd....

Table D1 (Continued):

S.No.	Property		Value	References
v)	Curie temperature, T_c		450°C	1
vi)	Anisotropy constant, K_1		3.25×10^5 J/m^2	6
vii)	Temperature coefficient of remanent magnetization		-0.2%/°C	2
viii)	Working point:	B	1000 gauss	2
		H	-850 Oe	2

*

1. J.Smit and H.P.J. Wijin, Ferrites, Philips Technical Library, Eindhover (1959) p. 177.

2. H. Kojima, Ferromagnetic Materials, Vol. 3, ed. E.P.Wohlfarth, North-Holland Publishing Company, 1982.

3. J.J. Went, G.W. Rathenau, E.W. Gorter and G.W. Van Osterhout, Phil. Tech. Rev., 13 (1952), 194.

4. F. Haberey, H.P.J. Wijin, Phys. Stat. Solidi, 26 (1968) 231.

5. K. Haneda, C. Miyakawa and H. Kojima, J. Amer. Ceramic Soc., 57 (1974a), 354.

6. B.T. Shrik and W.R. Buessem, J. Appl. Phys., 40 (1969), 1294.